Research Article

Tumoral hypoxic extracellular vesicles create a protective microenvironment for triple-negative breast cancer

Bianca C. Pachane[1,2*], Pedro H. T. Bottaro[1], Aline M. Machado[1], Cynthia A. de Castro[3], Gabriela Guerra[1], Larissa T. Gozzer[1,4], Marina M. Grigoli[5,6], Artur D. Zutião[5], Angelina M. Fuzer[5], Marcia R. Cominetti[5], Wanessa F. Altei[2,7], Heloisa S. Selistre-de-Araujo[1]

[1] Biochemistry and Molecular Biology Laboratory, Department of Physiological Sciences, Universidade Federal de São Carlos – UFSCar, São Carlos, SP, Brazil.
[2] Molecular Oncology Research Center, Barretos Cancer Hospital, Barretos, SP, Brazil.
[3] Pathology and Biocompatibility Laboratory, Department of Morphology and Pathology, Universidade Federal de São Carlos - UFSCar, São Carlos, SP, Brazil.
[4] Universidade de Aveiro, Aveiro, Portugal
[5] Department of Gerontology, Universidade Federal de São Carlos - UFSCar, São Carlos, SP, Brazil.
[6] Departament of Psychiatrie and Psychotherapie, University Medical Center Mainz, University of Johannes Gutenberg of Mainz – JGU, Mainz, Germany
[7] Radiation Oncology Department, Barretos Cancer Hospital, Barretos, SP, Brazil

[*] Corresponding author: Bianca Cruz Pachane. Department of Physiological Sciences, Universidade Federal de São Carlos – UFSCar, Rod. Washington Luis, km 235 – SP-310; 13565-905, São Carlos, SP, Brazil. biancapachane@gmail.com.

Conflict of Interest Statement: The authors declare no potential conflicts of interest.

ORCID:

BCP: 0000-0002-7302-4498
PHTB: 0000-0002-6456-6244
AMM: 0000-0001-8047-8482
CAC: 0000-0002-2675-8069
GG: 0009-0008-9975-1125
MMG: 0000-0002-8212-9574
ADZ: 0009-0005-8844-8866
AMF: 0000-0003-0673-8287
MRC: 0000-0001-6385-7392
WFA: 0000-0002-6636-7951
HSSA: 0000-0002-2372-7814

Graphical Abstract

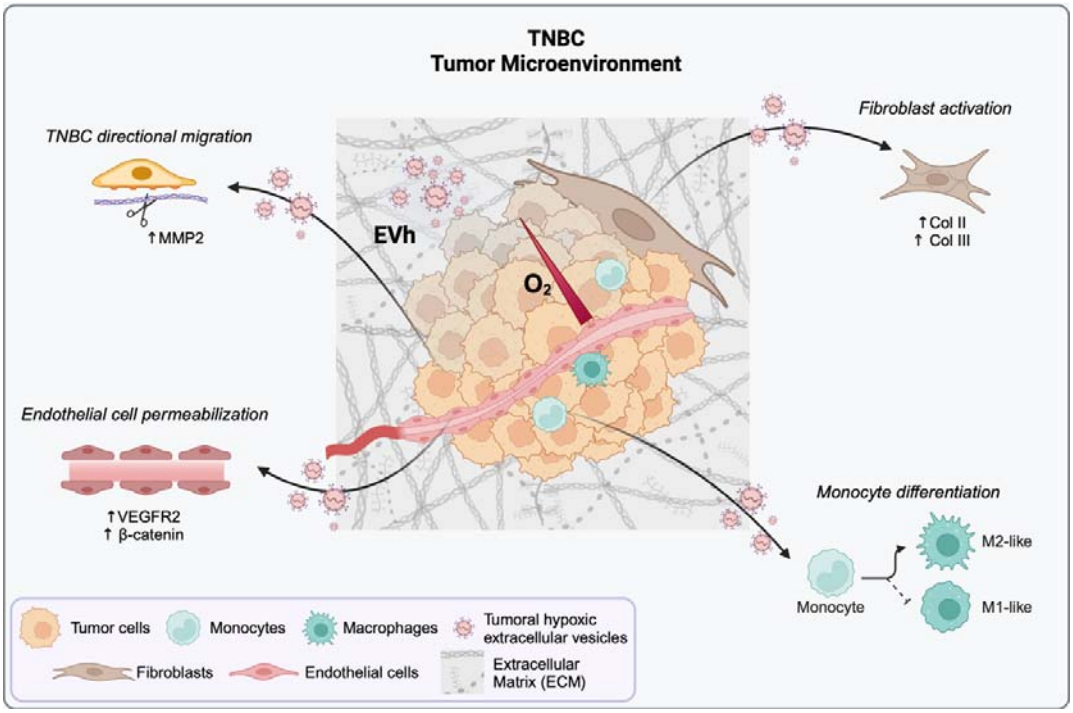

Abstract

Background: The highly metastatic triple-negative breast cancer (TNBC) relies on its tumor microenvironment (TME) to maintain phenotypic heterogeneity and progression. Extracellular vesicles from hypoxic TNBC were previously shown to aid tumoral invasion but their function in the tumor microenvironment is still unclear.

Methods: We used a novel method to investigate the TME *in vitro* called multicellular circulating co-culture, to characterize how TNBC-derived hypoxic EVs (EVh) interfere with tumoral and endothelial cells, fibroblasts, monocytes and macrophages.

Results: EVh promoted monocyte differentiation to M2-like macrophages and inhibited macrophage-derived phagocytosis in endothelial and tumoral cells. The protection of

endothelial, tumoral and stromal cellular integrity by EVh increased pro-tumoral and pro-angiogenic signaling, collagen matrix synthesis and a potential differentiation to cancer-associated fibroblasts.

Conclusion: Our findings highlighted the critical role of EVh in protecting tumor cells, indicating its cooperation towards a protective TME, which was demonstrated by the multicellular circulating co-culture and conventional co-culture protocols, leading to an adequate system with potential for investigating other tumor-related processes, including circulating tumor cells and metastasis.

Keywords: phagocytosis; extracellular vesicles; hypoxia; tumor microenvironment.

Background

Triple-negative breast cancer (TNBC) is mainly characterized by the lack of expression of receptors for estrogen, progesterone, and the human epidermal growth factor (HER2) (1). Comprised of a heterogeneous mass with a high risk of metastasis, TNBC affects over 15% of all breast tumors and presents poor overall survival (2). Its development is plagued with hypoxia, a condition in which oxygen distribution is reduced due to the increased cellular activity within the tumoral tissue, the inefficient tumoral vasculature, and the constant competition for nutrients within the mass (3,4). Hypoxia and tumorigenesis favor the secretion of extracellular vesicles (EV), nanoparticles (30-300 nm) released by all known cells with a major function in intercellular communication (5,6). Tumor-derived hypoxic EV (EVh) cargo has been previously described to favor pro-invasive pathways (7), but their direct action in the TNBC tumor microenvironment (TME) is still unknown.

The TME is a myriad of cellular and acellular components that evolve as the tumor phenotypic heterogeneity grows according to the stages of cancer progression (8–10). In the pre-invasive TME, autocrine signaling by epithelial (EGF), hepatocyte (HGF), and

transforming growth factors (TGF-β) favors cell proliferation, migration, and plasticity (11). The extracellular matrix (ECM) is modified mainly by fibroblasts called, in this context, cancer-associated fibroblasts (CAF) via protein synthesis and remodeling enzyme expression, which alters the protein content, activity and crosslinking to favor collagen synthesis and deposition (12,13). Pro-inflammatory mediators induce monocyte differentiation into macrophages and their subsequent polarization into tumor-associated macrophages (TAM) (13). The increased cell activity of the tumor stimulates the release of reactive oxygen species, which favors DNA damage and the secretion of pro-angiogenic stimuli including VEGF and fibroblast growth factor (FGF-2) (11). Once the invasive profile is achieved, cell motility is favored by the polarization of the cytoskeleton, the interplay between adhesion molecules, and ECM remodeling by matrix metalloproteases (MMPs) (14). These changes in cell behavior result from the secretion of TGF-β, interleukins (IL-6 and IL-8), and VEGF by CAFs, which favors the epithelial-mesenchymal transition, survival, and maintenance of immune control (11).

The collective complexity of the TME renders its study challenging, particularly when using *in vitro* techniques such as 2D cell culture. Due to the intrinsic method limitations, including the restriction in the number of simultaneous cell cultures and the low correspondence with the physiology of clinical TME, there has been a shift towards 3D cell culture models, which add a novel layer of complexity to *in vitro* studies. However, one pitfall of these models is the difficulty in observing individual cellular responses from the mass (15). In this work, we describe a novel method for studying the TME *in vitro* called the multicellular circulating co-culture (MC-CC) to determine how TNBC-derived hypoxic EVs influence individual immortalized cellular models in a TME setting. Using this approach, we demonstrated for the first time that EVh protects cells from macrophage-derived phagocytosis. This pro-tumorigenic function of EVh confirms previous suppositions on the tumoral function of EVs

and supports the development of novel EV-based strategies to overcome resistance to anticancer therapies.

Materials and Methods

Cell culture

Human cells from triple-negative mammary adenocarcinoma MDA-MB-231 (ATCC® CRM-HTB-26™) were grown between passages 36 and 45 in Leibovitz L-15 10% FBS media at 37 ºC. Dermal fibroblasts HDFa (ATCC® PCS-201-012™) and umbilical cord endothelial cells HUVEC (ATCC® CRL-1730™) were maintained between passages 6 and 15 in DMEM 10% FBS 1% pen/strep at 37 ºC, 5% CO_2. Monocytes THP-1 (ATCC® TIB-202™) were kept under suspension in RPMI 1640 10% FBS 1% pen/strep at 37 ºC, 5% CO_2. Cells were grown under sterile conditions for no longer than 4 weeks after thawing and were frequently tested for *Mycoplasma* using the MycoAlert® Assay kit (Lonza).

EVh separation and characterization

EVs from MDA-MB-231 cells grown in hypoxia (1% O_2) in EV-depleted media were separated and characterized as described previously (7), following the MISEV2023 guidelines (16). EVh samples were characterized by nanoparticle tracking analysis, transmission electron microscopy, protein quantification and Western blotting.

Nanoparticle Tracking Analysis (NTA)

EVh samples were diluted in PBS (1:1000, v/v) and injected in the module of a Nanosight NS300 (Malvern). Capture settings were set at camera level 16, slide shutter 1300, slider gain 512, FPS 25.0, and 749 frames, acquired in three-60s events. Analysis was performed on NTA software (v. 3.2 Dev Build 3.2.16) using the detect threshold of 4.

Transmission Electron Microscopy (TEM)

An EVh dilution (1:2, v/v in PBS) was deposited in copper grids covered with formvar and carbon (Lot 051115, 01800 F/C, 200 mesh Cu, Ted Pella Inc.) for 20 min, RT. Samples were fixed in 2% paraformaldehyde (PFA-PBS) for 20 min at RT and washed extensively in deionized water. Grids were exposed to 4% Uranyl-acetate (pH 4) and 2% methylcellulose solution for 10 min on ice and in the dark. Samples were airdried and visualized in an FEI TECNAI G2 F20 HRTEM microscope on 40,000x magnification.

Protein quantification

In 96-well plates, EVh samples were lysed with 2% SDS and diluted in deionized water (4:150). An albumin standard curve with known values (0-16 µg.ml) was created in parallel. Using the microBCA kit (Thermo-Fisher Scientific), a working solution was prepared (25A:24B:1C) and mixed with samples for 2 hours at 37 ºC for 2 hours. Plates were read at $O.D._{562nm}$ and quantification was considered successful if $R^2 < 0.99$.

Western blotting

EV samples (10 µl) were mixed with Laemmli buffer under reducing (1:4, v/v) and boiled at 100 ºC for 5 minutes. MDA-MB-231 cell lysates were used as control samples and Precision Plus Protein Dual-Color (Bio-Rad) was used as loading control. Samples were added to 10% SDS-PAGE gels for electrophoresis at 100 V. Gel proteins were transferred to nitrocellulose membranes (0.45 µm, Bio-Rad) at 100V, 4 ºC, for 2.5 hours in buffer (2.5 mM Tris, 2 M glycine, 20% methanol; pH 7.6) and confirmed by staining with Ponceau S. Membranes were blocked with 5% milk-TBST for 1 hour under agitation and probed overnight for ALIX (1:1000, 186429, Abcam), Calnexin (1:1000, mAb 2679, Cell Signaling), CD63 (1:1000, 59479, Abcam) or Flotillin-1 (1:1000, 61020, BD Biosciences). After three 5-minute washes with TBST, membranes were incubated with respective secondary antibodies (Goat anti-Rb, 1:15.000, #205718, Abcam; or Goat anti-Ms, 1:10.000, #97040, Abcam) for 1 hour at RT

under agitation. Membranes were washed four times with PBST for 5 minutes and exposed to ECL substrates (Clarity™ Western ECL Substrate, Bio-Rad and SuperSignal™ West Femto, Thermo-Fisher Scientific) for 2 minutes. Chemiluminescence reaction was documented using ChemiDoc™ XRS+ (Bio-Rad) and membranes cropped on the ImageLab software (Bio-Rad).

Monocyte differentiation in macrophages

Using OptiMEM 1% pen/strep (Gibco), THP-1 cells were seeded ($6x10^5$ cells/ml) in 6-well plates and treated with vehicle control (PBS), EVh (10^9 particles/ml) or phorbol-12-myristate-13-acetate (PMA, 100 nM) (17). Cell differentiation was evaluated with time-lapse light microscopy (Lux2, CytoSMART) with hourly snaps taken for 72h at 37 ºC, 5% CO_2 (18). Cell tracking was assessed using the TrackMate plugin from FIJI (18,19). Cell supernatant was collected and evaluated for IL-6, IL-10, TNF-α, and IL-1β with ELISA.

Time-lapse cell motility assay

In a 24-well dish, MDA-MB-231 ($5x10^4$ cells/ml), HUVEC ($5x10^4$ cells/ml) or HDFa (10^4 cells/ml) were seeded in complete growth media for adhesion over 24h at 37 ºC, 5% CO_2, followed by media replacement with OptiMEM 1% pen/strep. THP-1 cells were diluted in OptiMEM to achieve a 10^5 cells/ml concentration. An untreated group was maintained parallel to an EVh-treated group (10^9 particles/ml) for 24h at 37 ºC, 5% CO_2, under time-lapse light microscopy (Lux2, CytoSMART). Snaps were taken every 30 minutes and single-cell tracking was processed using the *TrackMate* plugin in FIJI (18,19).

Fluorescent gelatin invasion assay

Black 96-well plates coated with fluorescein-conjugated gelatin (0.2 mg/ml, G13187, Molecular Probes) were used to seed MDA-MB-231, HUVEC, HDFa or THP-1 cells in growth media. Plates were incubated overnight at 37 ºC, 5% CO_2. Media was substituted to OptiMEM 1% pen/strep containing EVh (10^9 particles/ml) or PBS for 24h at 37 ºC, 5% CO_2.

Cell viability, morphology, and gelatin degradation were assessed following the full protocol (20).

Cell viability assay

Cells seeded for invasion assays were mixed with a 10% resazurin solution (0.1 ml/ml, #199303, Sigma-Aldrich) in OptiMEM and incubated for 4h at 37 ºC, 5% CO_2, alongside a blank no-cell control and a 100%-reduced control. The supernatant was transferred to a new plate and analyzed by fluorescence (λ_{Exc} 555 nm, λ_{Em} 585 nm; SpectraMax i3, Molecular Devices).

Gelatin invasion in direct co-culture

MDA-MB-231, HUVEC, HDFa, or THP-cells were stained either with CellTracker™ Red CMTPX (5 µM, C34552, Invitrogen) or CellTrace™ CSFE (5 µM, C34554, Invitrogen) in OptiMEM. Two cell lineages were simultaneously seeded in a gelatin-coated 96-well black plate, treated with EVh (10^9 particles/ml) or PBS, and incubated at 37 ºC, 5% CO_2 for 24h. Cell viability, morphology, and gelatin degradation were determined following the full protocol (21).

Cell invasion in transwell co-culture

MDA-MB-231 cells previously attached to gelatin-coated coverslips were assembled in Boyden chambers with inserts containing a monolayer of HUVEC or HDFa cells. The system was maintained in OptiMEM for 24h at 37 ºC, 5% CO_2. Cells and conditioned media were processed following the full protocol (22).

Multicellular circulating co-culture (MC-CC)

MDA-MB-231, HUVEC, and HDFa cells were seeded to gelatin, Matrigel, and FN-coated coverslips, respectively, overnight at 37 ºC, 5% CO_2 and assembled in sterile QV500 (*Kirkstall*) culture chambers with 1 ml of OptiMEM 1% pen/strep. THP-1 cells were pre-

stained with CellTracker™ Red CMTPX (5 µM, C34552, Invitrogen) and transferred to the reservoir containing EVh (10^9 particles/ml) or vehicle (PBS). The tubing system was closed and connected to the MDA-MB-231, HUVEC, and HDFa chambers, propelled by a peristaltic pump set to a 50 µl/s flow rate. The circuit was incubated at 37 ºC, 5% CO_2 for 24h. Coverslips and the conditioned media were processed following the full protocol (23).

Individual static and circulating culture controls

Cells seeded in ECM-coated coverslips (23) were assembled individually in a sterile QV500 (*Kirkstall*) culture chamber with 1 ml of OptiMEM 1% pen/strep and connected with the tubing system to a reservoir containing 13 ml of media. Following the previous method, the system was maintained with a peristaltic pump, parallel to a static individual control. Coverslips were removed from the compartments, counterstained, and imaged at 40x magnification (ImageXpress Micro XRS, Molecular Devices). Cell circularity index and gelatin degradation were quantified using FIJI (7,18).

Enzyme-Linked Immunosorbent Assay - ELISA

High-affinity microplates were sensitized with monoclonal anti-cytokine antibodies (IL-6: 555220; IL-10: 555157; TNF-α: 555212; IL-1β: 557953, OptEIA, BD Biosciences) for 16-18h. Plates were washed thrice (0.05% Tween 20-PBS), incubated in 4% FBS-PBS for 1 hour at RT, and washed again. Both samples and the standard curve of recombinant cytokines were added to the wells for 2h, RT, and excess was washed off. Anti-cytokine antibodies conjugated with peroxidase were incubated for 1.5h, RT, followed by five washes with 0.05% Tween 20. A developing solution (3,3',5,5'-tetramethylbenzidine, TMB) was added to wells and the reaction was stopped with sulfuric acid. Plates were evaluated by spectrophotometry ($O.D._{450nm}$; SpectraMax i3, Molecular Devices). Sample concentrations

were calculated from the titration curve of the cytokine standards, and final concentrations were expressed in pg/ml.

Statistical analysis

Cellular assays were repeated on three distinct occasions in technical triplicates. MC-CC was repeated four times with both groups running simultaneously. Each sample was applied twice on zymograms, and average band densitometry was used for statistics. Datasets were checked for outliers using ROUT's test and distribution by Shapiro-Wilk ($n < 9$) or D'Agostino-Pearson omnibus K2 ($n \geq 9$). Parametric data was evaluated using unpaired t-tests (2 groups) or ANOVA one-way with Tukey's multiple comparison test (3+ groups). Non-parametric data was analyzed using the Mann-Whitney test (2 groups) or Kruskal-Wallis analysis of variance with Dunn's multiple comparison test (3+ groups). Values of $p < 0.05$ were considered statistically relevant (GraphPad Prism (v. 9.3)).

Results

EVh characterization

The isolation of EVh samples followed a previous method, where samples were thoroughly characterized (7). Incorporating the recommendations outlined in the MISEV2023 guidelines (16), EVh samples were separated from 2.2×10^7 MDA-MB-231 cells grown in hypoxia in serum-free media, leading to a population with modal size of 130.2 nm (± 78.7) and concentration of 3.69×10^{11} particles/ml (± 8.74×10^{10}) (Fig. 1A). Samples contained 236.6 µg/ml of protein and yielded 167,346.94 particles per cell or 1.07×10^{-5} µg protein per cell. Known EV biomarkers CD63 and flotillin-1 were abundant in EV samples, whereas Alix was faintly identified, and calnexin was absent (Fig. 1B). Visualization by TEM confirmed EVh abundance and typical morphology (Fig. 1C).

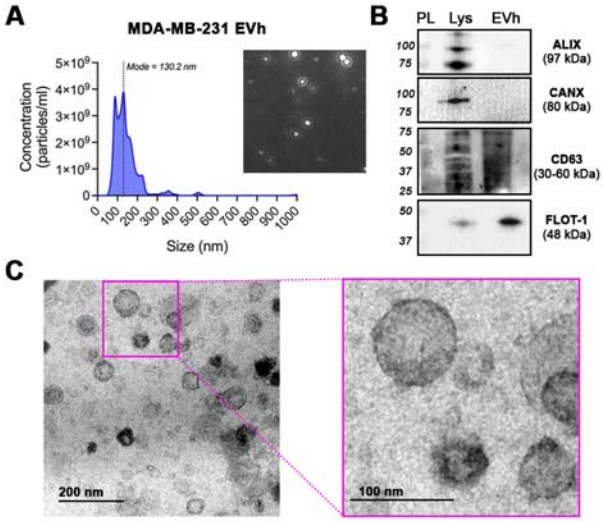

Figure 1. EVh characterization. (A) Size dispersion and EV abundance by nanoparticle tracking analysis of MDA-MB-231-derived EVh. (B) Detection of ALIX, calnexin (CANX), CD63 and flotillin-1. (C) Wide-field and close-up TEM images of EVh. Scale bars: 200 nm and 100 nm.

EVh mediates THP-1 differentiation into M2-like macrophages

The adherent phenotype of THP-1 cells was detected in both EVh- and PMA-treated groups after 16-24 hours of treatment, while untreated cells remained in suspension for up to 72 h (Fig. 2A and Suppl. 1A,B). The distinct cell morphologies found in EVh- and PMA- treated groups suggest alternative differentiation mechanisms (Fig. 2B). Gelatin invasion decreased upon EVh treatment (Fig. 2C,D). However, cell viability and circularity remained unchanged (Fig. 2E,F). The tracking of cell movement showed the undirected motility in untreated and PMA-differentiated cells, whereas a directional migration of EVh-differentiated cells was observed with higher mean speed and average distance traveled (Fig. 2G-I). Inflammatory cytokine profiling of THP-1 conditioned media detected TNF-α and IL-1β only in the PMA group (Fig. 2J,K), a non-significant trend of IL-6 reduction in the EVh group (Fig. 2L), and continuity of IL-10 expression in all three groups (Fig. 2M).

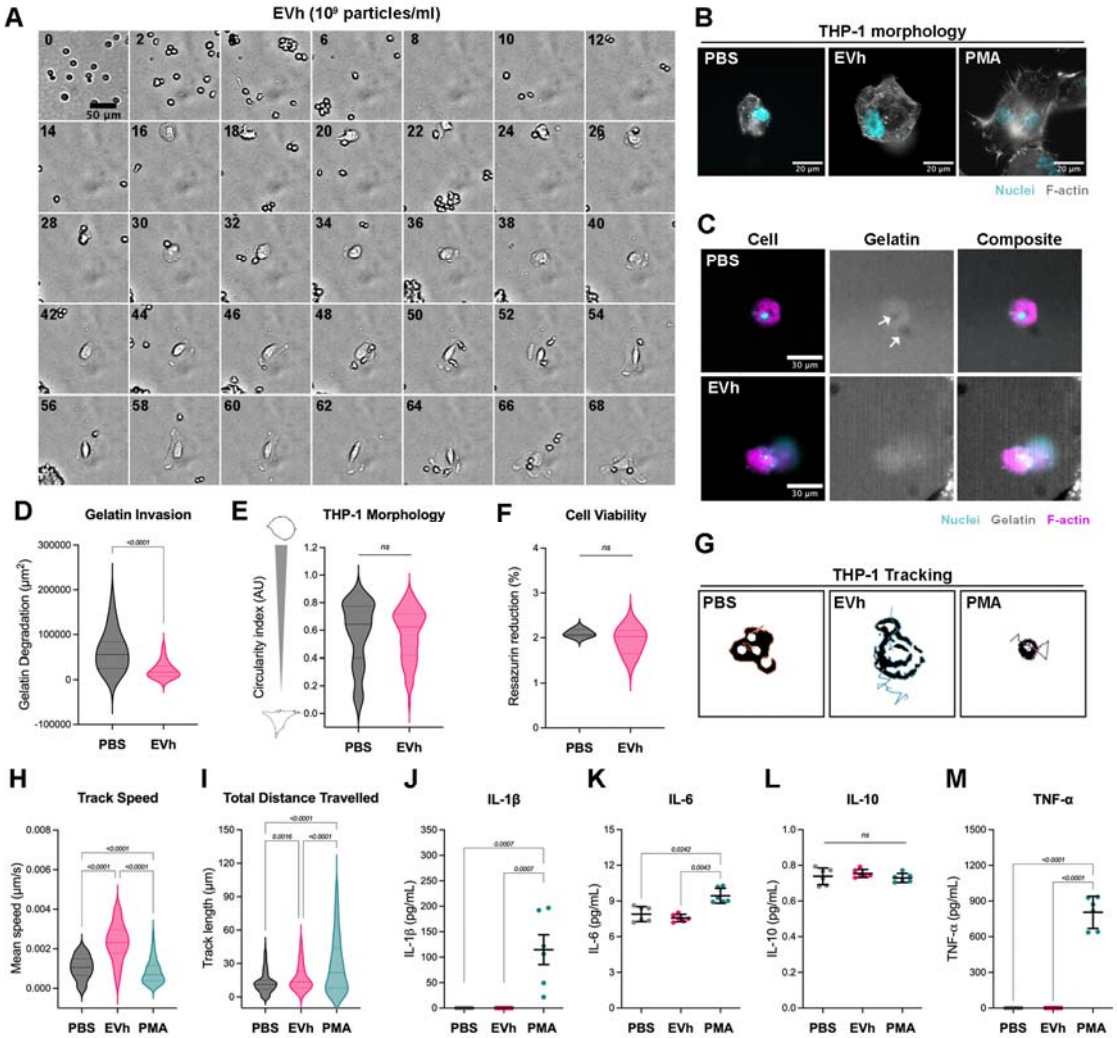

Figure 2. EVh-mediated macrophage differentiation. **A** - Timelapse tracking of THP-1 cells treated with EVh. Snaps from the same site were compiled in 2-hour increments over 3 days (scale bar: 50 µm). **B –** Representative images of THP-1 treated with vehicle (PBS), EVh or PMA after 72h differentiation (nuclei in cyan and F-actin in gray; scale bar: 20 µm). **C –** Representative images of THP-1 cells (nuclei in cyan, F-actin in magenta) treated with PBS or EVh on a gelatin coating (gray), with degradation spots identified by white arrows (scale bar: 30 µm). **D –** Quantification of degraded gelatin area (µm^2). **E** - Cell circularity index for quantification of THP-1 morphology. **F** - Cell viability of cells under invasion assay. **G –** Tracking of THP-1 trajectory over 24h. **H –** Average track speed of cells in 24 h (µm/s). **I** - Total distance traveled by cells in 24 h (µm). **J-M** - Quantification of cytokines TNF-α, IL-1β, IL-6, and IL-10, respectively. Assays were repeated over three different occasions with technical duplicates or triplicates. *p* values indicated above comparative bars with statistical significance.

Tumoral reprogramming of endothelial cells in vitro

EVh treatment in HUVEC promoted gelatin invasion and elongated cell morphology, consistent with the invasive phenotype (Fig. 3A-C). Cell viability was unaffected (Fig. Suppl. 2A). Unlike THP-1, there was non-directional motility in EVh-exposed HUVEC (Fig. 3D). Although the average speed of movement was similar between the groups, a higher distance traveled by cells was seen in EVh groups (Fig. 3E,F).

The pro-tumoral effect of EVh in endothelial cells was further investigated using indirect and direct co-culture assays with MDA-MB-231 cells. In indirect co-culture, where tumor cells were separated from endothelial cells by an insert (Fig. 3G), HUVEC exhibited typical morphology and significant intercellular interaction, while the tumoral cells showed multiple cytoskeleton extensions, which gave them a downy appearance (Fig. 3H). In EVh-treated conditions, the cytoskeleton retracted as endothelial cells visibly lost intercellular interactions, and tumor cells showed a more elongated phenotype, without F-actin extensions (Fig. 3I). Tumoral gelatin invasion was detected in both co-culture groups, likely due to MMP-2 activation (Fig. 3J-K; Suppl. Fig. 2B). Both MMP-2 activity and gelatin degraded area were slightly higher in EVh-treated groups (Fig. 3L). Adding to previous results (7), we found EVh directs movement in MDA-MB-231, which facilitates tumoral invasion in gelatin matrices (Fig. Suppl. 2C-E).

In the direct co-culture approach, where both cells were seeded in the same well simultaneously (Fig. 3M), the proximity between cells led to a stress response in which the endothelial cytoskeleton turned to a star-shape, while tumoral cells became more cohesive (Fig. 3N). Once exposed to EVh, cells recapitulated their original morphological characteristics (Fig. 3N; Suppl. Fig. 2F,G). These changes were reflected in the circularity index, suggesting the importance of EVh in the regulation of intercellular interactions on the

TME (Fig. 3O). Like the indirect co-culture model, EVh-treated cells also increased gelatin invasion (Fig. 3P-Q). In this scenario, cell viability remained unchanged (Fig. 3R).

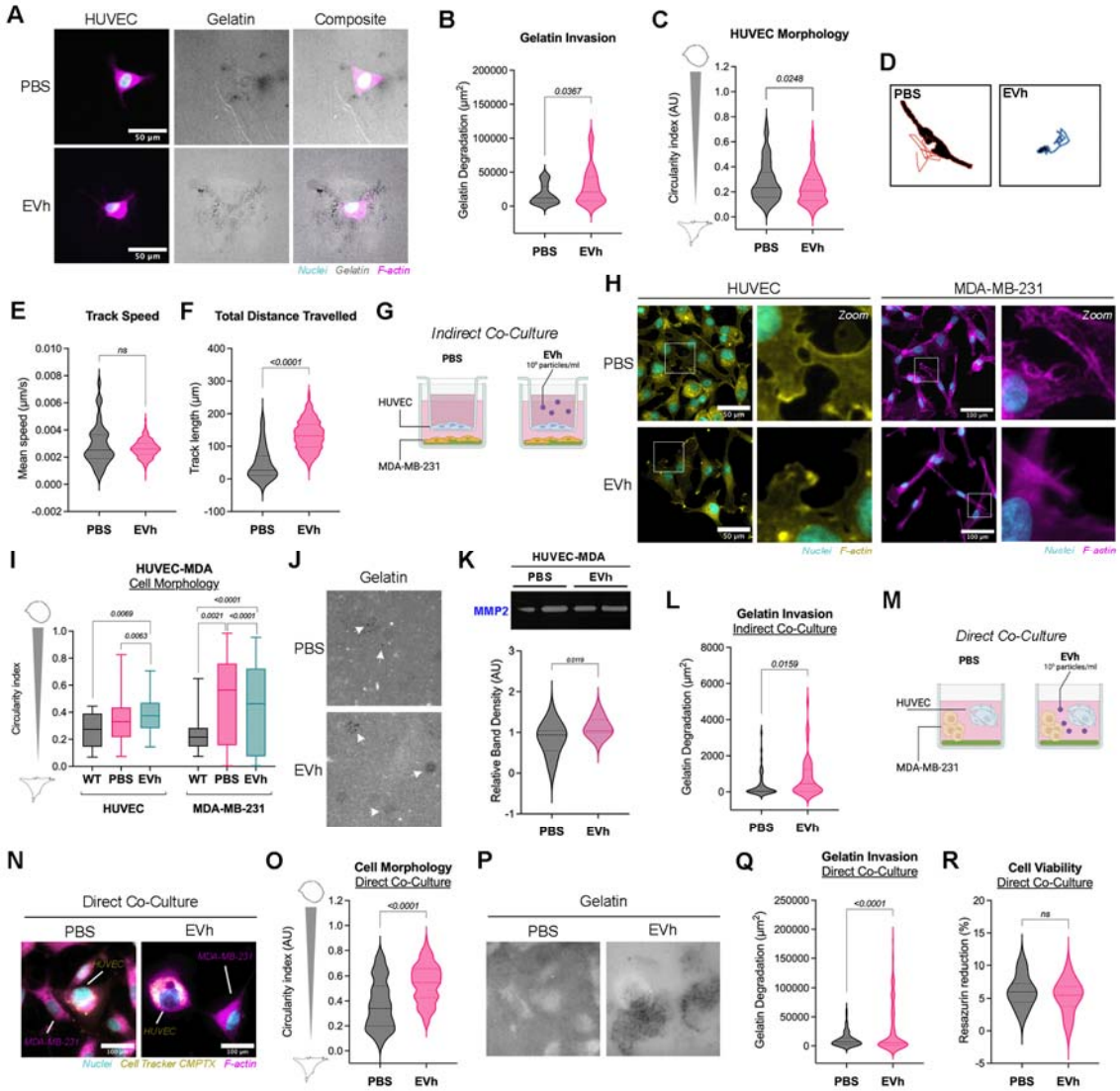

Figure 3. Endothelial cells respond to tumoral signaling. **A -** Representative images of HUVEC (nuclei in cyan, F-actin in magenta) treated with PBS or EVh on a gelatin coating (gray), with degradation spots in black (scale bar: 50 µm). **B –** Quantification of degraded gelatin area (µm^2) in individual HUVEC cultures. **C –** HUVEC circularity index in individual culture. **D -** Tracking of HUVEC trajectory over 24h. **E –** Average track speed of cells in 24 h (µm/s). **F -** Total distance traveled by cells in 24 h (µm). **G –** Experimental design of the indirect co-culture assay. **H –** Representative images of HUVEC (nuclei in cyan, F-actin in yellow; scale bar: 50

µm) in indirect co-culture with MDA-MB-231 (nuclei in cyan, F-actin in magenta; scale bar: 100 µm). **I –** Cell circularity index for quantification of HUVEC and MDA-MB-231 morphology in direct co-culture. **J –** Representative images of gelatin matrix (gray) with degradation spots identified by white arrows. **K -** MMP-2 detection by gelatin zymography and densitometry analysis of indirect co-culture. **L –** Quantification of degraded gelatin area (μm^2) in indirect co-culture. **M -** Experimental design of the direct co-culture assay. **N –** Representative images of HUVEC (cytoplasm in yellow) in direct co-culture with MDA-MB-231 (nuclei in cyan, F-actin in magenta) seeded atop a gelatin coating (gray) (scale bar: 100 µm). **O -** Cell circularity index for quantification of combined cell morphology in direct co-culture. **P -** Quantification of degraded gelatin area (μm^2) in direct co-culture. **Q –** Cell viability of HUVEC and MDA-MB-231 direct co-culture. Assays were repeated on three different occasions with technical triplicates. *p* values indicated above comparative bars with statistical significance.

Fibroblast subtle response to tumor cells and EVh

HDFa promoted visible gelatinase activity, especially after EVh administration (Fig. 4A). Fibroblasts showed a migratory phenotype and increased gelatin degradation, coupled with a significant rise in cell viability after EVh exposure (Fig. 4B-D). HDFa movement was polarized and resulted from reduced track speed and increased total distance traveled (Fig. 4E-G).

To evaluate the responses of HDFa in different models of tumoral association, then an indirect co-culture assay was assembled between fibroblasts and gelatin-seeded MDA-MB-231. There was a subtle fibroblast response to tumoral signaling, regardless of EVh exposure (Fig. 4H-I). Cell area was reduced, making them broader than the individual cell controls, and tumoral gelatin degradation remained unchanged (Fig. 4J-K). The cell circularity index supported these observations. Zymograms suggest MMP-2 activity is reduced by EVh exposure (Fig. 4L). EVh also favors anti-invasive behaviors in a direct co-culture model. Both cells show a visibly distinct phenotype (Fig. 4M, Suppl. Fig. 2H), the overall cell

morphology is more circular (Fig. 4N), gelatin degradation is reduced after EVh administration (Fig..4O) and cell viability remains unchanged (Suppl. Fig. 2I).

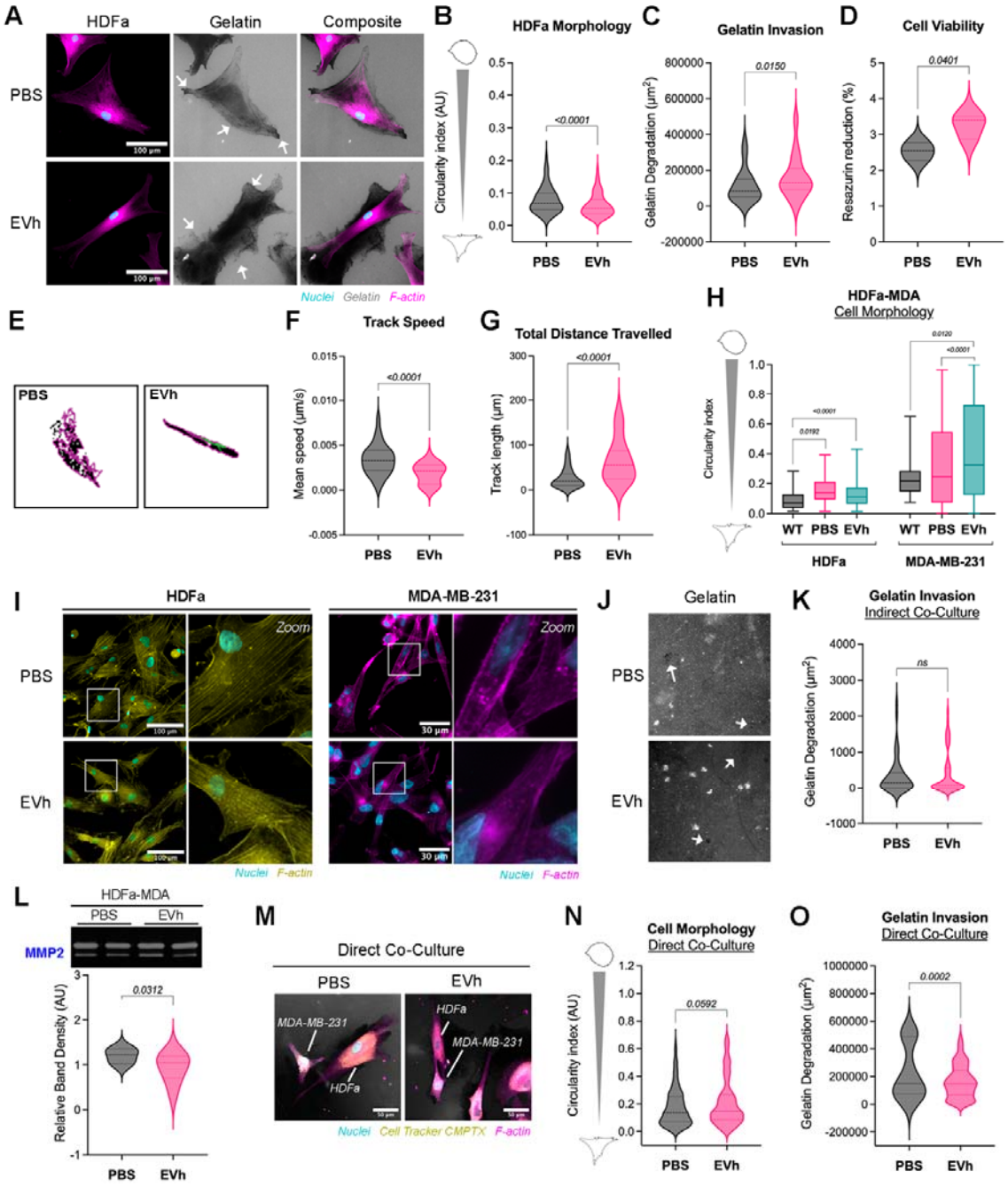

Figure 4. Fibroblast response to tumoral signaling. **A** - Representative images of HDFa (nuclei in cyan, F-actin in magenta) treated with PBS or EVh on a gelatin coating (gray), with degradation spots identified by white arrows (scale bar: 100 µm). **B** – Cell circularity index for quantification of HDFa morphology in individual culture. **C** - Quantification of degraded gelatin area (µm^2) in individual HUVEC cultures. **D** – HDFa

cell viability in individual culture. **E -** Tracking of HDFa trajectory over 24h. **F –** Average track speed of cells in 24 h (µm/s). **G -** Total distance traveled by cells in 24 h (µm). **H –** Representative images of HDFa (nuclei in cyan, F-actin in yellow; scale bar: 100 µm) in indirect co-culture with MDA-MB-231 (nuclei in cyan, F-actin in magenta; scale bar: 30 µm). **I –** Cell circularity index for quantification of HDFa and MDA-MB-231 morphology in indirect co-culture. **J -** Representative images of gelatin matrix (gray) with degradation spots identified by white arrows. **K -** Quantification of degraded gelatin area (μm^2) in indirect co-culture. **L –** MMP-2 detected by gelatin zymography and densitometry analysis to identify gelatinase activity in indirect co-culture. **M –** Representative images of MDA-MB-231 (cytoplasm in yellow) in direct co-culture with HDFa (nuclei in cyan, F-actin in magenta) seeded atop a gelatin coating (gray) (scale bar: 100 µm). **N -** Cell circularity index for quantification of combined cell morphology in direct co-culture. **O –** Quantification of degraded gelatin area (μm^2) in direct co-culture. Assays were repeated on three different occasions with technical triplicates. *p* values indicated above comparative bars with statistical significance.

EVh inhibits phagoptosis via macrophages in the TME

A multicellular circulating co-culture (MC-CC) was developed to recreate the cellular complexity of a TNBC tumor *in vitro* for evaluating EVh response in a TME-like setting (Fig. 5A). In the system, each TME cell type was seeded in a compartment for individual assessment of targets, while maintaining communication by a constant flow of 50 µl/s, set by previous optimization steps containing isolated cells (Fig. Suppl. 3A). A closed system comprised of MDA-MB-231, HUVEC, HDFa and THP-1 cells circulated for 24 hours showed high levels of phagoptosis (i.e., death by macrophage phagocytosis) (24), especially in the TNBC and endothelial cell chambers (Fig. 5B). In these chambers, integer nuclei and cytoplasm were seldomly found. EVh exposure led to more frequently sighted cells with integer nuclei and cytoplasm throughout chambers, suggesting phagoptosis inhibition. Cell morphological plasticity was confirmed by the circularity indexes of MDA-MB-231 and HUVEC (Fig. Suppl. 3B-C). The media flow reduced gelatin invasion in TNBC cells compared to individual static controls. EVh treatment partially recovered the cell invasive ability (Fig. 5C). The conditioned media was tested for gelatinases, and MMP-2 activity

remained unchanged (Fig. 5D, Suppl. 3D). Cytokine IL-1β was present in similar levels in both groups, but IL-6 was more abundant in the EVh-treated system (Fig. 5E,F).

Pro-tumoral components were quantified based on immunofluorescence images. In endothelial cells, the expression of β-catenin and VEGFR2 expression, which are involved in intercellular junctions and the angiogenic cascade, respectively, was higher in EVh groups (Fig. 5G,H). In fibroblasts, where cell integrity was best maintained among all cell types, subtle morphological differences were found (Fig. Suppl. 4E). Regarding ECM deposition, their expression of collagen type II and III was increased by EVh treatment, located mostly around the cellular body (Fig. 5I,J). Due to technical restraints, collagen type I was not investigated.

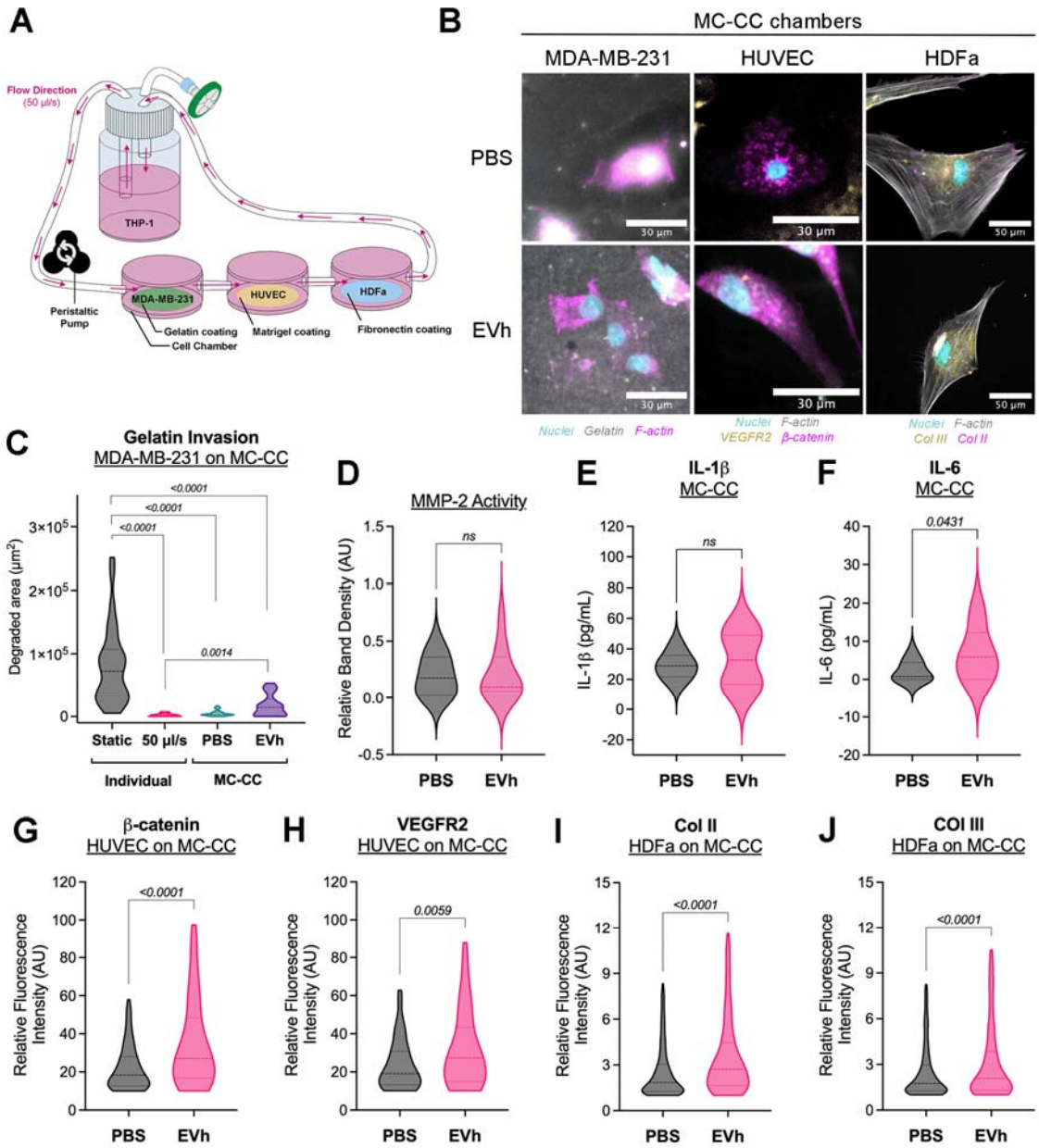

Figure 5. EVh inhibits phagoptosis in the TME. **A –** Experimental design of the multicellular circulating co-culture assay (MC-CC) using the QV500 system (Kirstall). **B -** Representative images of MC-CC chambers containing MDA-MB-231, HUVEC or HDFa treated with PBS or EVh. (scale bars: 30 µm and 50 µm). **C -** Quantification of degraded gelatin area (µm^2) in the MC-CC MDA-MB-231 chamber. **D –** Band densitometry of MMP-2 detected by gelatin zymography from the MC-CC conditioned media. **E,F –** Cytokines IL-1β and IL-6 probed from the MC-CC conditioned media by ELISA. **G,H –** Relative fluorescence intensity of β-catenin and

VEGFR2 in HUVEC, respectively. **I,J –** Relative fluorescence intensity of collagen II and III in HDFa, respectively. Assays were repeated on four different occasions with a single replicate. *p* values indicated above comparative bars with statistical significance.

Interestingly, most macrophages in the MC-CC were identified within the MDA-MB-231 chamber (Fig. 6A). THP-1 was less frequently sighted in EVh-treated groups than in the controls, reinforcing our hypothesis that EVh protects the TME from phagoptosis. A direct co-culture with each cell line was executed to check individual responses to THP-1 with EVh treatment, leading to similar results. We found high levels of phagoptosis in both MDA-MB-231 and HUVEC wells, and cell debris were also found in fibroblasts (Fig. 6B). EVh treatment partially inhibited macrophage activity and recapitulated the original phenotype in all cell types. A corona of THP-1 cells attached to the fibroblasts was observed, suggesting that both cells may exchange information. In this case, fibroblasts became broader, branched, and more polarized, suggesting their activation (Fig. 6C). Cell viability was unchanged by EVh in all three settings (Fig. Suppl. 3F), but treatment increased gelatin invasion in tumor and endothelial cells upon direct culture with THP-1 and decreased in fibroblasts (Fig. 6D).

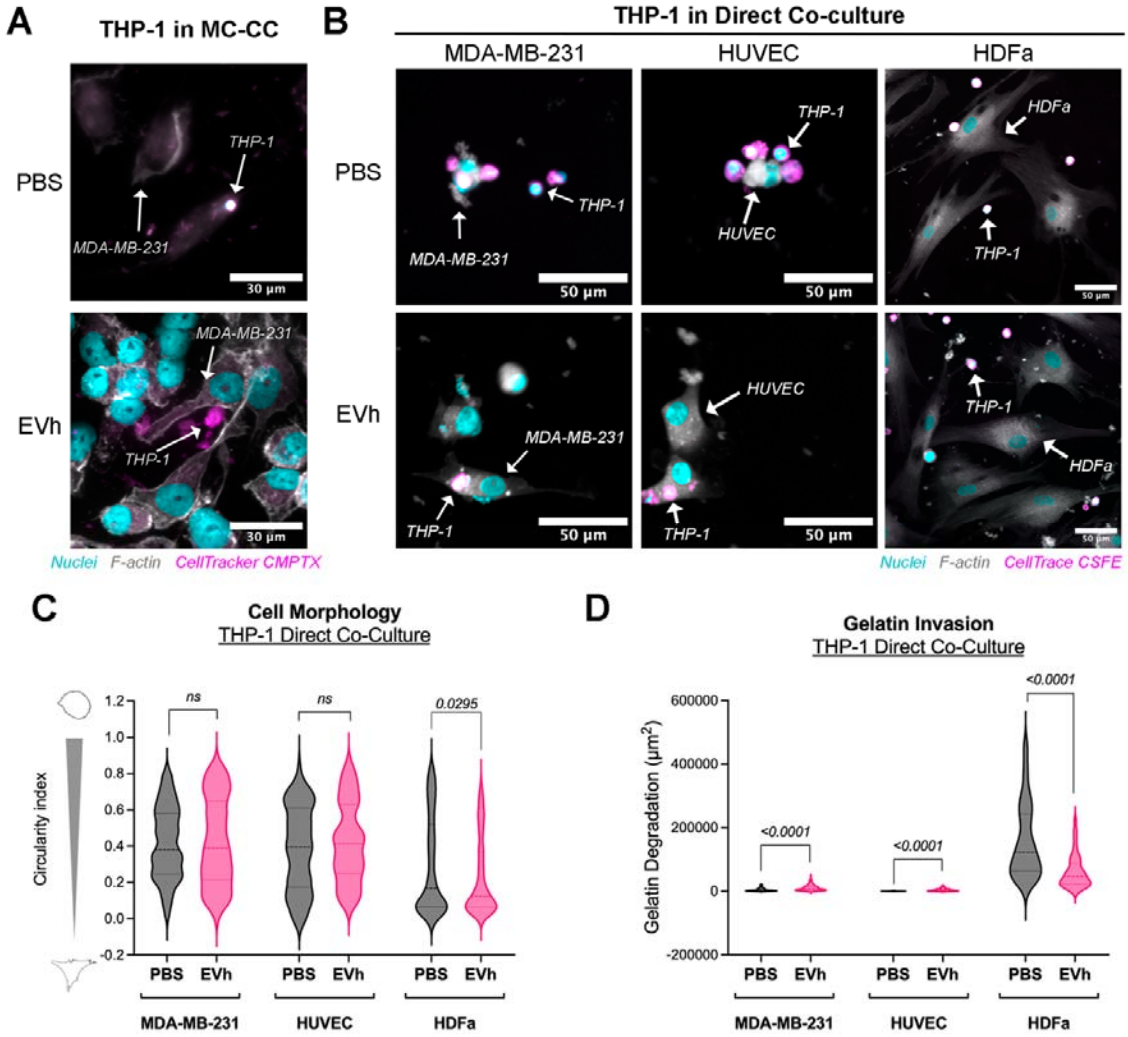

Figure 6. Macrophage remodeling by EVh in TME models *in vitro* A – Representative images of THP-1 (magenta, stained with CellTracker CMPTX) attachment to MDA-MB-231 MC-CC chambers (nuclei in cyan, F-actin in gray; scale bar: 30 µm). **B -** Representative images of THP-1 cells (magenta, stained with CellTrace CSFE) in direct co-culture with MDA-MB-231, HUVEC or HDFa (nuclei in cyan, F-actin in gray; scale bars: 50 µm). **C -** Cell circularity index for quantification of combined cell morphology in THP-1 direct co-culture with MDA-MB-231, HUVEC and HDFa. **D –** Quantification of degraded gelatin area (μm^2) in THP-1 direct co-culture with MDA-MB-231, HUVEC and HDFa. Assays were repeated on three different occasions with technical triplicates. *p* values indicated above comparative bars with statistical significance.

Discussion

The role of EVs in tumor progression and development is well described, and as new facets of tumorigenesis are revealed, their importance to cancer continuity becomes apparent. Tumor-associated EVs have been implicated in promoting angiogenesis (25), immune modulation (26), tumoral invasion (7,27), migration (28) and organotropic metastasis (29). The establishment of hypoxia in tumor progression promotes EV secretion in breast cancer, with distinct composition and characteristics (5–7). After describing the pro-invasive potential of hypoxic EV in comparison to normoxic EVs from TNBC cell line MDA-MB-231 (7), we show in this work that EVh differentiated THP-1 cells in M2-like macrophages, downregulating phagoptosis in tumor microenvironment models *in vitro*. Moreover, under the MC-CC model, EVh protected endothelial and tumoral cellular integrity, promoted pro-tumoral responses in endothelial cells and induced collagen synthesis in fibroblasts.

Monocyte recruitment and activation are crucial steps of the tumor-induced immune cascade, often triggered by the macrophage colony-stimulating factor (M-CSF) and other environmental cues (30). The differentiation of monocytes to macrophages *in vitro* relies on PMA to generate non-polarized cells, which may be induced to a pro-inflammatory M1 phenotype or an anti-inflammatory M2 profile, each with a distinct cytokine secretion pattern (17,31). We found that PMA-induced cells were enriched with pro-inflammatory components IL-1β, IL-6 and TNF-□, suggesting an M1-like profile, and the subtle reduction in IL-6 and sustained expression of anti-inflammatory IL-10 suggested that EVh promoted an M2-like phenotype (31–34).

The macrophage profiles were consistently maintained during co-culture with tumoral and endothelial cells, where phagoptosis was abundant in the control groups but avoided with EVh treatment. Cell death by phagocytosis results from the imbalance between the eat me and don’t eat me signals from the target cell and their recognition by receptors in the phagocytic cell (24). In our models, EVh likely modulated don’t eat me signals, such as

CD47 and MHC-I, to improve cell survival, corroborating previous findings in which hypoxia inhibited macrophage phagocytosis in a HIF-1 -dependent manner (35,36). Further studies are required to confirm this hypothesis.

Studying the TME *in vitro* is challenging due to methodological, practical, and technological limitations. The recent development of techniques such as multicellular co-cultures, microfluidics and 3D culture has improved the complexity with which we can investigate basic mechanisms (37–39). A significant limitation of multicellular 3D co-cultures is the difficulty of evaluating responses in individual cells from the cultured mass, which often relies upon more refined and less accessible techniques (15). To circumvent this issue, we described a novel method to study the TME *in vitro* where cells are cultured *in tandem* in a commercially available system, henceforth named a multicellular circulating co-culture (MC-CC). Results obtained from the MC-CC model were complementary to other co-culture techniques, including direct and indirect co-culture, but we have not investigated whether it is a better alternative to 3D culture. This method was previously described for studying the blood-brain barrier but has several limitations, including the number of available co-culture chambers, flow shear force, and lack of direct contact between chambers which reduces our ability to evaluate certain cellular responses (40). We acknowledge that different experimental designs, including other cell types, order of chambers, incubation conditions, flow rate, and media composition, may interfere with the results and have not been investigated in the present study.

Our experimental design permitted the evaluation of cell morphology alongside cytokine and enzyme secreted in the circulating medium across all MC-CC chambers. EVh cause stromal and tumor cells to favor a more pro-tumoral phenotype, likely due to the increased levels of IL-6, a cytokine whose overexpression is closely related to the development of various tumors, regulation of the acute phase of inflammation, and modulation of T and B

lymphocytes (41). Furthermore, the high levels of IL-6 and IL-1β favor the inflammatory phenotype of cancer-associated fibroblasts, which is consistent with our evaluation of fibroblast response (42). There was a non-statistical tendency for an increase in IL-1β levels in EVh-treated cells, suggesting fibroblast activation, but additional testing to detect differences in □-smooth muscle actin (□-SMA) is required to confirm this supposition.

EVh in endothelial cells under MC-CC increased the expression of markers for cell-cell adhesion and proangiogenicity, including VEGFR2 and β-catenin (43). This may facilitate tumor development and metastatic spread by increasing the connections between endothelial and tumoral cells and encouraging angiogenesis (43,44). Intercellular junctions are crucial for endothelial integrity and depend on the function of multiple proteins, especially VE-cadherin (45). With nearly exclusive expression in vascular endothelium, VE-cadherin is intracellularly linked to β-catenin, which directly connects to the cytoskeleton (46,47). In the indirect co-culture assay, we could not identify which adhesive molecules were influenced by EVh; however, multicellular co-culture under flow suggested an increase in β-catenin expression in HUVEC under EVh action. These conflicting results hint the tumor microenvironment is essential for maintaining endothelial intercellular adhesions but require additional investigation. Furthermore, we suggest that EVh disrupts endothelial cell adhesion to aid EVh-mediated tumor cell invasion.

Fibroblasts are structural support cells that can associate with tumors, transforming into cancer-associated fibroblasts (CAFs) through prolonged tumor-associated inflammation (TAI) signaling (42). TAI is sustained by continuous tumor mass growth and hypoxia, which have been described as determinants of the inflammatory phenotype of fibroblasts in pancreatic cancer (48). EVh increased fibroblast activity, modified their morphology and, in MC-CC, promoted the synthesis of type II and type III collagen, Both collagens are fibrillar and associated with increased ECM stiffness, a crucial factor for metastasis (49). Hypoxic

extracellular vesicles also play a significant role in modulating fibroblast activity, leading to increased production of collagen types II and III. This process of extracellular matrix remodeling through MMP production and excessive collagen formation has been shown to promote tumor growth, progression, and resistance to treatments such as radiotherapy (43,44,50,51). In this setting, we show that hypoxic extracellular vesicles from triple-negative breast cancer impact fibroblast activity.

In summary, we found that tumor-derived hypoxic EVs show a distinct immune-modulating function, allowing the differentiation of M2-like macrophages in a TNBC in the TME *in vitro* and inhibiting endothelial and tumoral phagoptosis. EVh administration protected the endothelial and tumoral cellular integrity from phagoptosis. It promoted pro-tumoral and pro-angiogenic responses in endothelial cells, inducing collagen synthesis in fibroblasts and their potential differentiation to CAFs. In addition, our work describes a novel method for studying the TME *in vitro* using a commercial system with great potential for investigating other tumor-related processes, including circulating tumor cells and metastasis.

Author's contribution

BCP: Conceptualization; Data curation; Formal Analysis; Funding acquisition; Investigation; Methodology; Project administration; Software; Writing – original draft. PHTB: Formal Analysis; Investigation; Visualization; AMM: Formal Analysis; Investigation; Writing – review & editing; CAC: Formal Analysis; Investigation; Methodology; Writing – review & editing; GG: Investigation; Visualization; LTG: Methodology; Visualization; MMG: Investigation; Writing – review & editing; ADZ: Investigation; Visualization; AMF: Conceptualization; Resources; Writing – review & editing; MRC: Funding acquisition; Resources; Software; Writing – review & editing; WFA: Conceptualization; Resources;

Supervision; Writing – review & editing; HSSA: Conceptualization; Funding acquisition; Resources; Supervision; Writing – review & editing.

Acknowledgments

The authors thank members from LMBBM and LABEN for critical advice. We thank the Laboratory of Structural Characterization (LCE/DEMa/UFSCar) for the electron microscopy facilities; Otavio Thiemann and Glaucius Oliva (IFSC/USP) for Beckman ultracentrifuge and rotors; Fausto Bruno dos Reis Almeida for the use of Nanosight NS300; Monica Rosa da Costa Iemma for the HDFa cell lineage; Gerson Jhonatan Rodrigues and Luis Henrique Oliveira de Moraes for the HUVEC cell lineage.

Data availability

The data generated in this study are available within the article and its supplementary data files. Raw files are available upon reasonable request to the corresponding author. Detailed protocols have been submitted to the “protocols.io” platform (20–23). We have submitted all relevant data of our EV experiments to the EV-TRACK knowledgebase (EV-TRACK ID: EV240149) (52). This study does not contain artificial intelligence-generated data.

Funding

This work was funded by the São Paulo Research Foundation through grants 2019/05149-9, 2021/01983-4, and 2022/04146-9 (to BCP); 2022/12307-2 (to PHTB); 2020/11328-0 (to LTG); 2017/01287-2 (to AMF); 2021/01863-9 and 2021/14673-3 (to MRC); 2019/11437-7 (to HSSA); Coordenação de Aperfeiçoamento de Pessoal de Nível Superior (CAPES), code 001; and Conselho Nacional de Desenvolvimento Científico e Tecnológico (CNPq) through grants 143120/2023-9 (ID 1618, to GG); 174872/2023-2 (to AMF). The funding agencies had no direct involvement in the study's design, conduct, analysis, or reporting.

References

1. Foulkes William D., Smith Ian E., Reis-Filho Jorge S. Triple-Negative Breast Cancer. New England Journal of Medicine. 2010;363(20):1938–48.

2. Altei WF, Pachane BC, Souza C, Marques MMC, Selistre-de-Araújo H. New insights into the discovery of drugs for triple-negative breast cancer metastasis. Expert Opinion on Drug Discovery. 2022 Apr 3;17(4):365–76.

3. Majmundar AJ, Wong WJ, Simon MC. Hypoxia-Inducible Factors and the Response to Hypoxic Stress. Molecular Cell. 2010 Oct 22;40(2):294–309.

4. Zhang Y, Zhang H, Wang M, Schmid T, Xin Z, Kozhuharova L, et al. Hypoxia in Breast Cancer—Scientific Translation to Therapeutic and Diagnostic Clinical Applications. Front Oncol. 2021 Mar 11;11:652266.

5. King HW, Michael MZ, Gleadle JM. Hypoxic enhancement of exosome release by breast cancer cells. BMC Cancer. 2012 Sep 24;12(1):421.

6. Xu R, Rai A, Chen M, Suwakulsiri W, Greening DW, Simpson RJ. Extracellular vesicles in cancer — implications for future improvements in cancer care. Nat Rev Clin Oncol. 2018 Oct;15(10):617–38.

7. Pachane BC, Nunes ACC, Cataldi TR, Micocci KC, Moreira BC, Labate CA, et al. Small Extracellular Vesicles from Hypoxic Triple-Negative Breast Cancer Cells Induce Oxygen-Dependent Cell Invasion. International Journal of Molecular Sciences. 2022 Jan;23(20):12646.

8. Jin MZ, Jin WL. The updated landscape of tumor microenvironment and drug repurposing. Sig Transduct Target Ther. 2020 Aug 25;5(1):1–16.

9. Kucharzewska P, Belting M. Emerging roles of extracellular vesicles in the adaptive response of tumour cells to microenvironmental stress. Journal of Extracellular Vesicles. 2013;2(1):20304.

10. Dagogo-Jack I, Shaw AT. Tumour heterogeneity and resistance to cancer therapies. Nat Rev Clin Oncol. 2018 Feb;15(2):81–94.

11. Visser KE de, Joyce JA. The evolving tumor microenvironment: From cancer initiation to metastatic outgrowth. Cancer Cell. 2023 Mar 13;41(3):374–403.

12. Amos SE, Choi YS. The Cancer Microenvironment: Mechanical Challenges of the Metastatic Cascade. Front Bioeng Biotechnol [Internet]. 2021 Feb 12 [cited 2024 Apr 6];9. Available from: https://www.frontiersin.org/articles/10.3389/fbioe.2021.625859

13. Yuan Z, Li Y, Zhang S, Wang X, Dou H, Yu X, et al. Extracellular matrix remodeling in tumor progression and immune escape: from mechanisms to treatments. Molecular Cancer. 2023 Mar 11;22(1):48.

14. Hamidi H, Ivaska J. Every step of the way: integrins in cancer progression and metastasis. Nat Rev Cancer. 2018 Sep;18(9):533–48.

15. Dey M, Ayan B, Yurieva M, Unutmaz D, Ozbolat IT. Studying tumor angiogenesis and cancer invasion in a 3D vascularized breast cancer microenvironment. Adv Biol (Weinh). 2021 Jul;5(7):e2100090.

16. Welsh JA, Goberdhan DCI, O'Driscoll L, Buzas EI, Blenkiron C, Bussolati B, et al. Minimal information for studies of extracellular vesicles (MISEV2023): From basic to advanced approaches. Journal of Extracellular Vesicles. 2024;13(2):e12404.

17. Starr T, Bauler TJ, Malik-Kale P, Steele-Mortimer O. The phorbol 12-myristate-13-acetate differentiation protocol is critical to the interaction of THP-1 macrophages with Salmonella Typhimurium. PLoS One. 2018 Mar 14;13(3):e0193601.

18. Schindelin J, Arganda-Carreras I, Frise E, Kaynig V, Longair M, Pietzsch T, et al. Fiji: an open-source platform for biological-image analysis. Nat Methods. 2012 Jul;9(7):676–82.

19. Ershov D, Phan MS, Pylvänäinen JW, Rigaud SU, Le Blanc L, Charles-Orszag A, et al. TrackMate 7: integrating state-of-the-art segmentation algorithms into tracking pipelines. Nat Methods. 2022 Jul;19(7):829–32.

20. Pachane BC, Araujo HSS de. Fluorescent Gelatin Degradation Assay to Evaluate EVh Action in TME Cells. 2024 Sep 9 [cited 2024 Sep 16]; Available from: https://www.protocols.io/view/fluorescent-gelatin-degradation-assay-to-evaluate-dkt34wqn

21. Pachane BC, Araujo HSS de. Cell Invasion in Direct Co-Culture. 2024 Sep 9 [cited 2024 Sep 16]; Available from: https://www.protocols.io/view/cell-invasion-in-direct-co-culture-dkws4xee

22. Pachane BC, Araujo HSS de. Indirect Co-Culture Assay using Boyden Chambers. 2024 Sep 10 [cited 2024 Sep 16]; Available from: https://www.protocols.io/view/indirect-co-culture-assay-using-boyden-chambers-dkxc4xiw

23. Pachane BC, Bottaro PHT, Altei WF, Araujo HSS de. Multicellular Circulating Co-Culture. 2024 Sep 10 [cited 2024 Sep 16]; Available from: https://www.protocols.io/view/multicellular-circulating-co-culture-dkxv4xn6

24. Brown GC. Cell death by phagocytosis. Nat Rev Immunol. 2024 Feb;24(2):91–102.

25. Gao J, Zhang X, Jiang L, Li Y, Zheng Q. Tumor endothelial cell-derived extracellular vesicles contribute to tumor microenvironment remodeling. Cell Communication and Signaling. 2022 Jun 25;20(1):97.

26. Marar C, Starich B, Wirtz D. Extracellular vesicles in immunomodulation and tumor progression. Nat Immunol. 2021 May;22(5):560–70.

27. Hoshino D, Kirkbride KC, Costello K, Clark ES, Sinha S, Grega-Larson N, et al. Exosome Secretion Is Enhanced by Invadopodia and Drives Invasive Behavior. Cell Reports. 2013 Dec 12;5(5):1159–68.

28. Sung BH, von Lersner A, Guerrero J, Krystofiak ES, Inman D, Pelletier R, et al. A live cell reporter of exosome secretion and uptake reveals pathfinding behavior of migrating cells. Nat Commun. 2020 Apr 29;11(1):2092.

29. Hoshino A, Costa-Silva B, Shen TL, Rodrigues G, Hashimoto A, Tesic Mark M, et al. Tumour exosome integrins determine organotropic metastasis. Nature. 2015 Nov;527(7578):329–35.

30. Italiani P, Boraschi D. From Monocytes to M1/M2 Macrophages: Phenotypical vs. Functional Differentiation. Frontiers in Immunology. 2014 Oct 17;5:514.

31. Jayasingam SD, Citartan M, Thang TH, Mat Zin AA, Ang KC, Ch'ng ES. Evaluating the Polarization of Tumor-Associated Macrophages Into M1 and M2 Phenotypes in Human Cancer Tissue: Technicalities and Challenges in Routine Clinical Practice. Front Oncol. 2020 Jan 24;9:1512.

32. Kartikasari AER, Huertas CS, Mitchell A, Plebanski M. Tumor-Induced Inflammatory Cytokines and the Emerging Diagnostic Devices for Cancer Detection and Prognosis. Front Oncol [Internet]. 2021 Jul 7 [cited 2024 Apr 30];11. Available from: https://www.frontiersin.org/journals/oncology/articles/10.3389/fonc.2021.692142/full

33. Yeh CR, Slavin S, Da J, Hsu I, Luo J, Xiao GQ, et al. Estrogen receptor α in cancer associated fibroblasts suppresses prostate cancer invasion via reducing CCL5, IL6 and macrophage infiltration in the tumor microenvironment. Mol Cancer. 2016 Jan 20;15:7.

34. Yunna C, Mengru H, Lei W, Weidong C. Macrophage M1/M2 polarization. European Journal of Pharmacology. 2020 Jun 15;877:173090.

35. Anand RJ, Gribar SC, Li J, Kohler JW, Branca MF, Dubowski T, et al. Hypoxia causes an increase in phagocytosis by macrophages in a HIF-1alpha-dependent manner. J Leukoc Biol. 2007 Nov;82(5):1257–65.

36. Martins F, Oliveira R, Cavadas B, Pinto F, Cardoso AP, Castro F, et al. Hypoxia and Macrophages Act in Concert Towards a Beneficial Outcome in Colon Cancer. Cancers. 2020 Mar 28;12(4):818.

37. Casali BC, Baptista MP, Pachane BC, Cortez AA, Altei WF, Selistre-de-Araújo HS. Blockage of αvβ3 integrin in 3D culture of triple-negative breast cancer and endothelial cells inhibits migration and discourages endothelial-to-mesenchymal plasticity. Biochemistry and Biophysics Reports. 2024 Jul 1;38:101686.

38. Park JV, Chandra R, Cai L, Ganguly D, Li H, Toombs JE, et al. Tumor Cells Modulate Macrophage Phenotype in a Novel In Vitro Co-Culture Model of the NSCLC Tumor Microenvironment. J Thorac Oncol. 2022 Oct;17(10):1178–91.

39. Rebelo SP, Pinto C, Martins TR, Harrer N, Estrada MF, Loza-Alvarez P, et al. 3D-3-culture: A tool to unveil macrophage plasticity in the tumour microenvironment. Biomaterials. 2018 May 1;163:185–97.

40. Miranda-Azpiazu P, Panagiotou S, Jose G, Saha S. A novel dynamic multicellular co-culture system for studying individual blood-brain barrier cell types in brain diseases and cytotoxicity testing. Sci Rep. 2018 Jun 8;8(1):8784.

41. Weng YS, Tseng HY, Chen YA, Shen PC, Al Haq AT, Chen LM, et al. MCT-1/miR-34a/IL-6/IL-6R signaling axis promotes EMT progression, cancer stemness and M2

macrophage polarization in triple-negative breast cancer. Molecular Cancer. 2019 Mar 18;18(1):42.

42. Kennel KB, Bozlar M, De Valk AF, Greten FR. Cancer-Associated Fibroblasts in Inflammation and Antitumor Immunity. Clinical Cancer Research. 2023 Mar 14;29(6):1009–16.

43. Liu Y, Shi K, Chen Y, Wu X, Chen Z, Cao K, et al. Exosomes and Their Role in Cancer Progression. Front Oncol [Internet]. 2021 Mar 22 [cited 2024 Oct 21];11. Available from: https://www.frontiersin.org/journals/oncology/articles/10.3389/fonc.2021.639159/full

44. Becker A, Thakur BK, Weiss JM, Kim HS, Peinado H, Lyden D. Extracellular Vesicles in Cancer: Cell-to-Cell Mediators of Metastasis. Cancer Cell. 2016 Dec 12;30(6):836–48.

45. Duong CN, Vestweber D. Mechanisms Ensuring Endothelial Junction Integrity Beyond VE-Cadherin. Front Physiol [Internet]. 2020 May 21 [cited 2024 Jun 21];11. Available from: https://www.frontiersin.org/journals/physiology/articles/10.3389/fphys.2020.00519/full

46. Dejana E. Endothelial cell–cell junctions: happy together. Nat Rev Mol Cell Biol. 2004 Apr;5(4):261–70.

47. Guo M, Breslin JW, Wu MH, Gottardi CJ, Yuan SY. VE-cadherin and β-catenin binding dynamics during histamine-induced endothelial hyperpermeability. American Journal of Physiology-Cell Physiology. 2008 Apr;294(4):C977–84.

48. Mello AM, Ngodup T, Lee Y, Donahue KL, Li J, Rao A, et al. Hypoxia promotes an inflammatory phenotype of fibroblasts in pancreatic cancer. Oncogenesis. 2022 Sep 15;11(1):1–9.

49. Winkler J, Abisoye-Ogunniyan A, Metcalf KJ, Werb Z. Concepts of extracellular matrix remodelling in tumour progression and metastasis. Nat Commun. 2020 Oct 9;11(1):5120.

50. Chulpanova DS, Kitaeva KV, James V, Rizvanov AA, Solovyeva VV. Therapeutic Prospects of Extracellular Vesicles in Cancer Treatment. Front Immunol [Internet]. 2018 Jul 3 [cited 2024 Oct 21];9. Available from: https://www.frontiersin.org/journals/immunology/articles/10.3389/fimmu.2018.01534/full

51. Taghizadeh-Hesary F. “Reinforcement” by Tumor Microenvironment: The Seventh “R” of Radiobiology. International Journal of Radiation Oncology, Biology, Physics. 2024 Jul 1;119(3):727–33.

52. Van Deun J, Mestdagh P, Agostinis P, Akay Ö, Anand S, Anckaert J, et al. EV-TRACK: transparent reporting and centralizing knowledge in extracellular vesicle research. Nat Methods. 2017 Mar;14(3):228–32.

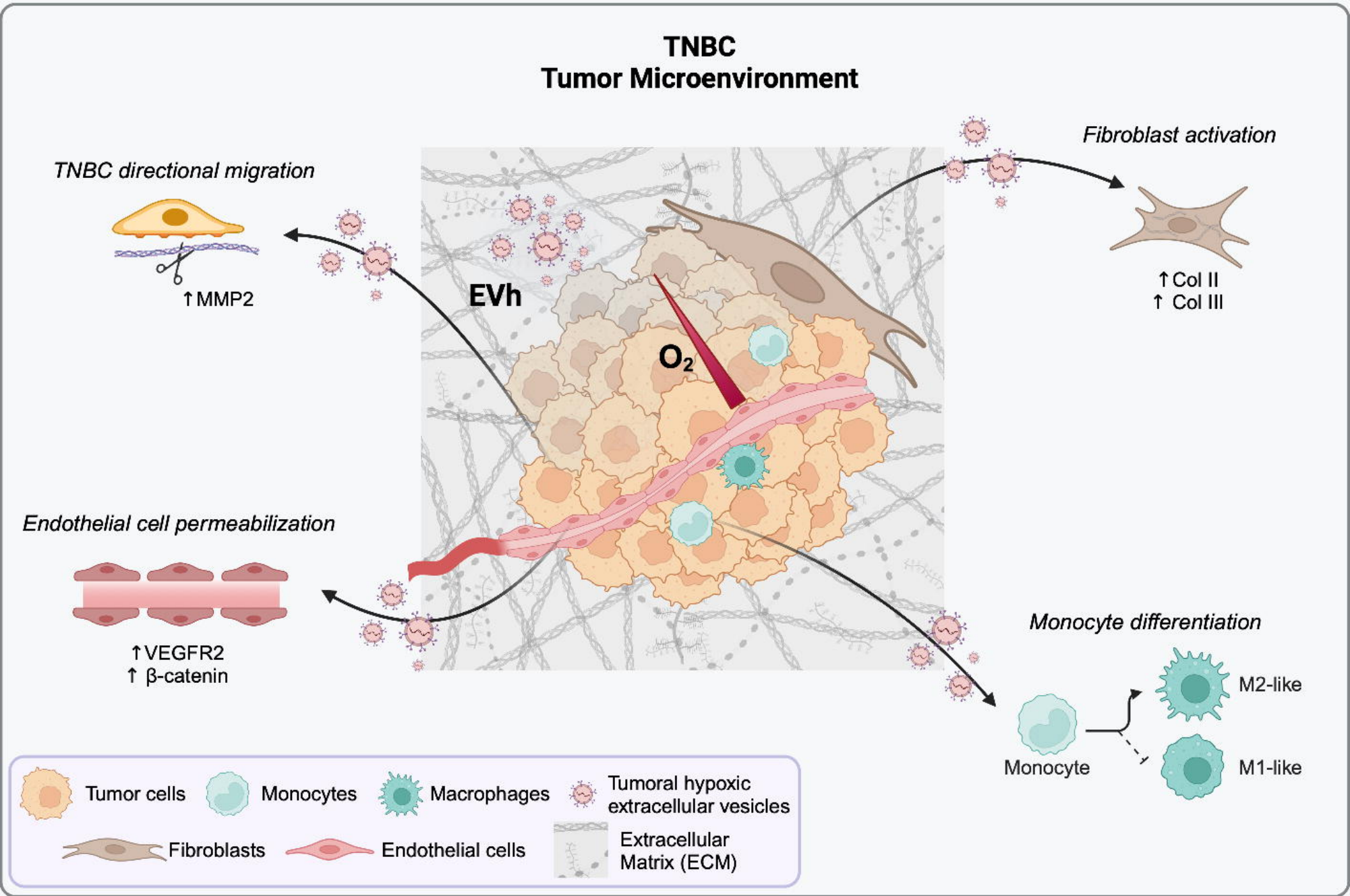
TNBC
Tumor Microenvironment
TNBC directional migration
↑MMP2
Fibroblast activation
↑Col II
↑ Col III
EVh
O_2
Endothelial cell permeabilization
↑VEGFR2
↑ β-catenin
Monocyte differentiation
Monocyte
M2-like
M1-like
Tumor cells
Monocytes
Macrophages
Tumoral hypoxic extracellular vesicles
Fibroblasts
Endothelial cells
Extracellular Matrix (ECM)

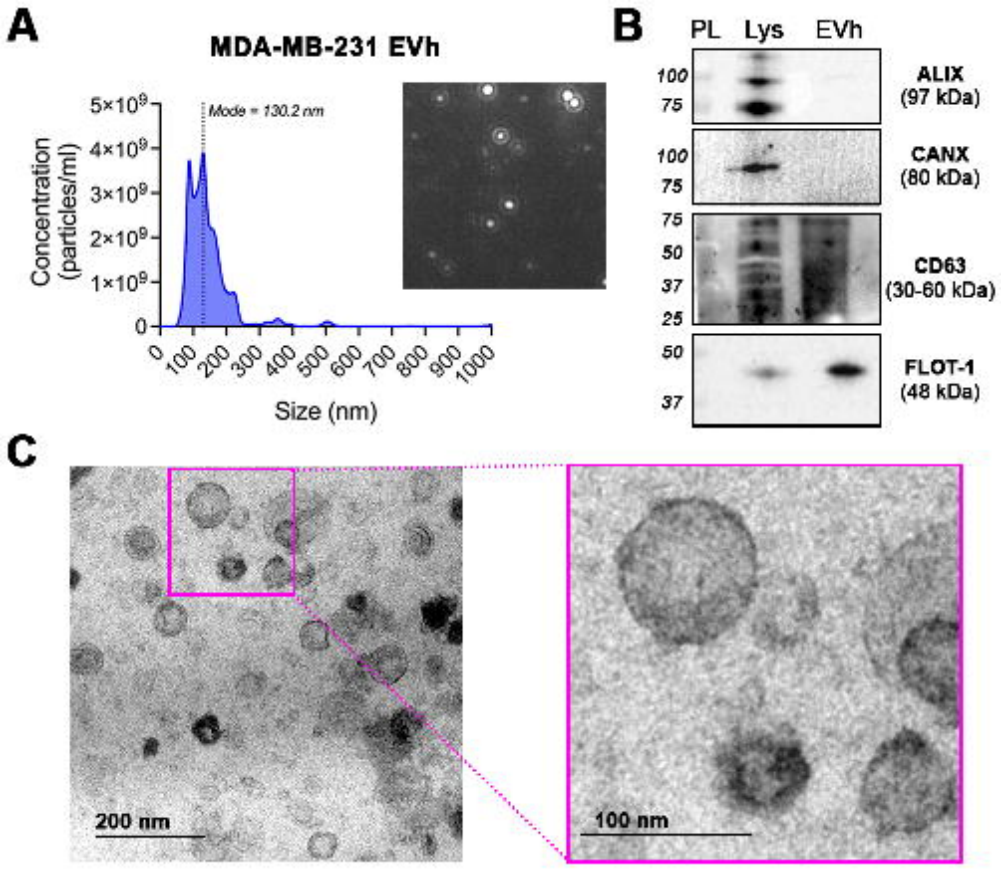
A
MDA-MB-231 EVh
Mode = 130.2 nm
Concentration (particles/ml)
5×10^9
4×10^9
3×10^9
2×10^9
1×10^9
0
0 100 200 300 400 500 600 700 800 900 1000
Size (nm)
B
PL Lys EVh
100
75
ALIX (97 kDa)
100
75
CANX (80 kDa)
75
50
37
25
CD63 (30-60 kDa)
50
37
FLOT-1 (48 kDa)
C
200 nm
100 nm

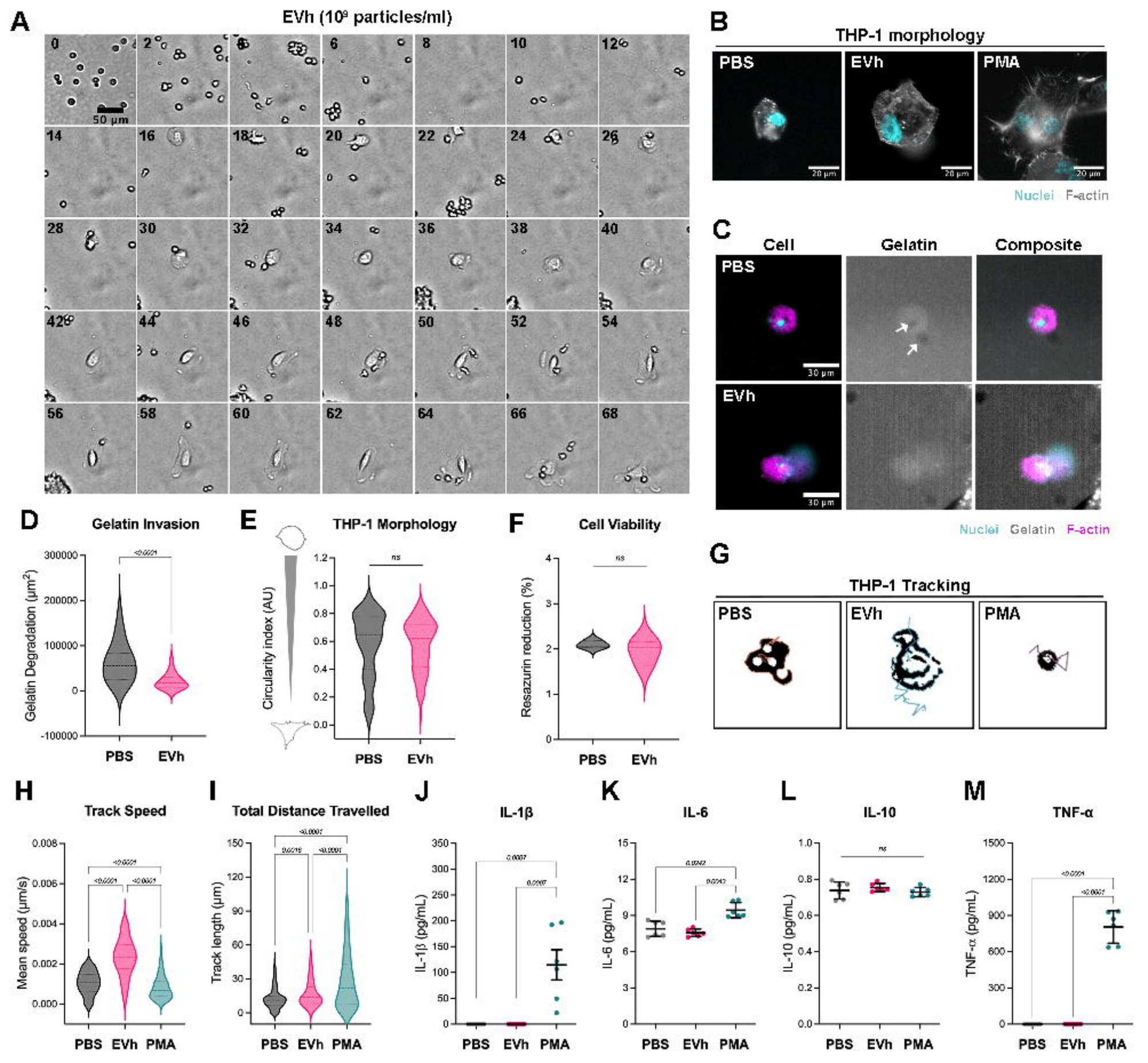
A
EVh (10⁹ particles/ml)
0
2
4
6
8
10
12
50 µm
14
16
18
20
22
24
26
28
30
32
34
36
38
40
42
44
46
48
50
52
54
56
58
60
62
64
66
68
B
THP-1 morphology
PBS
EVh
PMA
20 µm
Nuclei F-actin
C
Cell
Gelatin
Composite
PBS
EVh
30 µm
Nuclei Gelatin F-actin
D
Gelatin Invasion
Gelatin Degradation (µm²)
300000
200000
100000
0
-100000
PBS
EVh
E
THP-1 Morphology
Circularity index (AU)
1.2
1.0
0.8
0.6
0.4
0.2
0.0
ns
PBS
EVh
F
Cell Viability
Resazurin reduction (%)
4
3
2
1
0
ns
PBS
EVh
G
THP-1 Tracking
PBS
EVh
PMA
H
Track Speed
Mean speed (µm/s)
0.008
0.006
0.004
0.002
0.000
PBS
EVh
PMA
I
Total Distance Travelled
Track length (µm)
150
120
90
60
30
0
PBS
EVh
PMA
J
IL-1β
IL-1β (pg/mL)
350
300
250
200
150
100
50
0
PBS
EVh
PMA
K
IL-6
IL-6 (pg/mL)
15
12
9
6
3
0
PBS
EVh
PMA
L
IL-10
IL-10 (pg/mL)
1.0
0.8
0.6
0.4
0.2
0.0
ns
PBS
EVh
PMA
M
TNF-α
TNF-α (pg/mL)
1500
1200
900
600
300
0
PBS
EVh
PMA

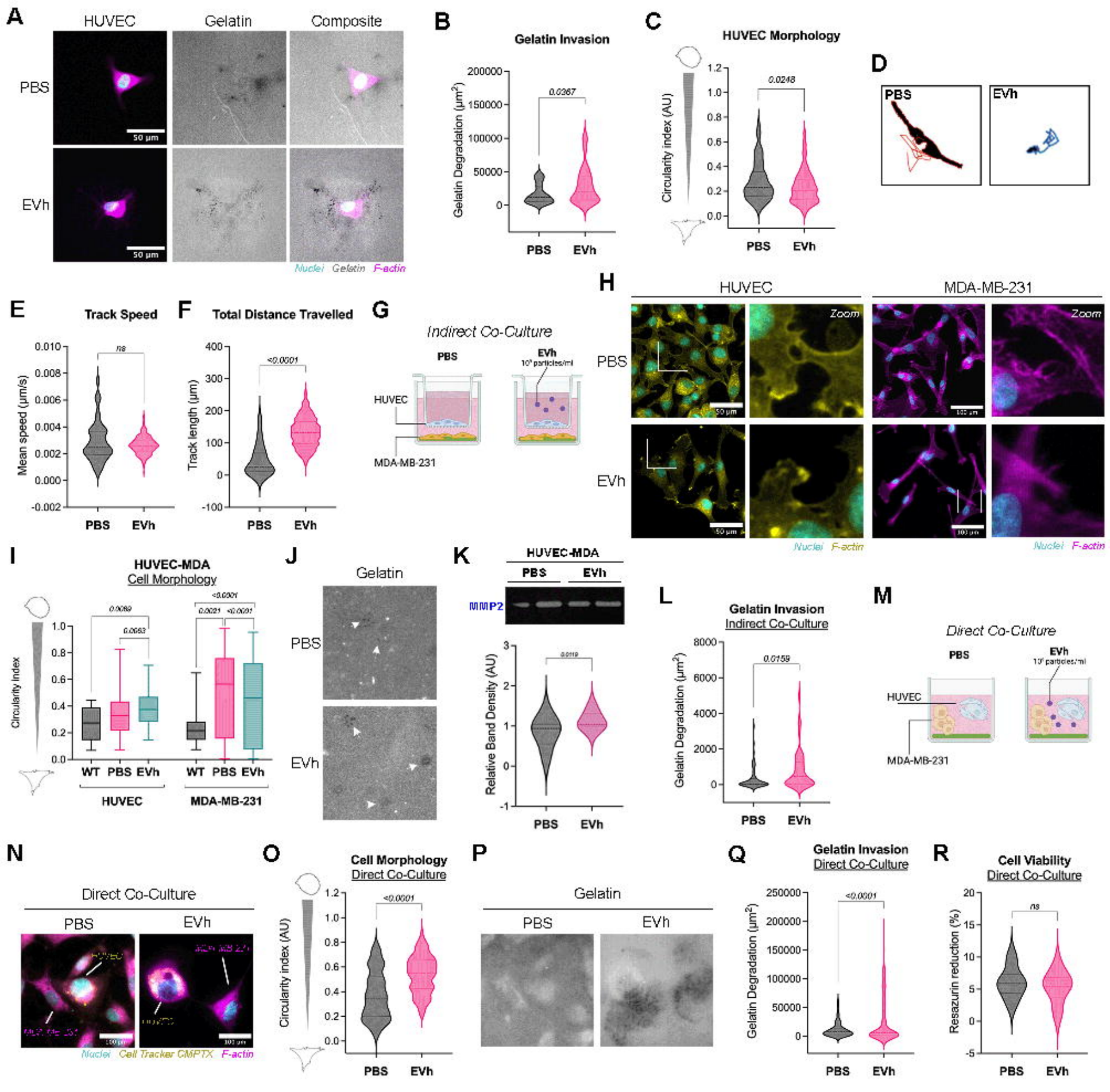
A
HUVEC
Gelatin
Composite
PBS
EVh
50 µm
Nuclei Gelatin F-actin
B
Gelatin Invasion
Gelatin Degradation (µm²)
0.0367
PBS EVh
C
HUVEC Morphology
Circularity index (AU)
0.0248
PBS EVh
D
PBS
EVh
E
Track Speed
Mean speed (µm/s)
ns
PBS EVh
F
Total Distance Travelled
Track length (µm)
<0.0001
PBS EVh
G
Indirect Co-Culture
PBS
EVh
10⁵ particles/ml
HUVEC
MDA-MB-231
H
HUVEC
MDA-MB-231
PBS
EVh
Zoom
Nuclei F-actin
I
HUVEC-MDA
Cell Morphology
Circularity Index
0.0089
0.0063
<0.0001
0.0021
<0.0001
WT PBS EVh
WT PBS EVh
HUVEC
MDA-MB-231
J
Gelatin
PBS
EVh
K
HUVEC-MDA
PBS EVh
MMP2
Relative Band Density (AU)
0.0119
PBS EVh
L
Gelatin Invasion
Indirect Co-Culture
Gelatin Degradation (µm²)
0.0159
PBS EVh
M
Direct Co-Culture
PBS
EVh
10⁵ particles/ml
HUVEC
MDA-MB-231
N
Direct Co-Culture
PBS
EVh
Nuclei Cell Tracker CMPTX F-actin
O
Cell Morphology
Direct Co-Culture
Circularity index (AU)
<0.0001
PBS EVh
P
Gelatin
PBS
EVh
Q
Gelatin Invasion
Direct Co-Culture
Gelatin Degradation (µm²)
<0.0001
PBS EVh
R
Cell Viability
Direct Co-Culture
Resazurin reduction (%)
ns
PBS EVh

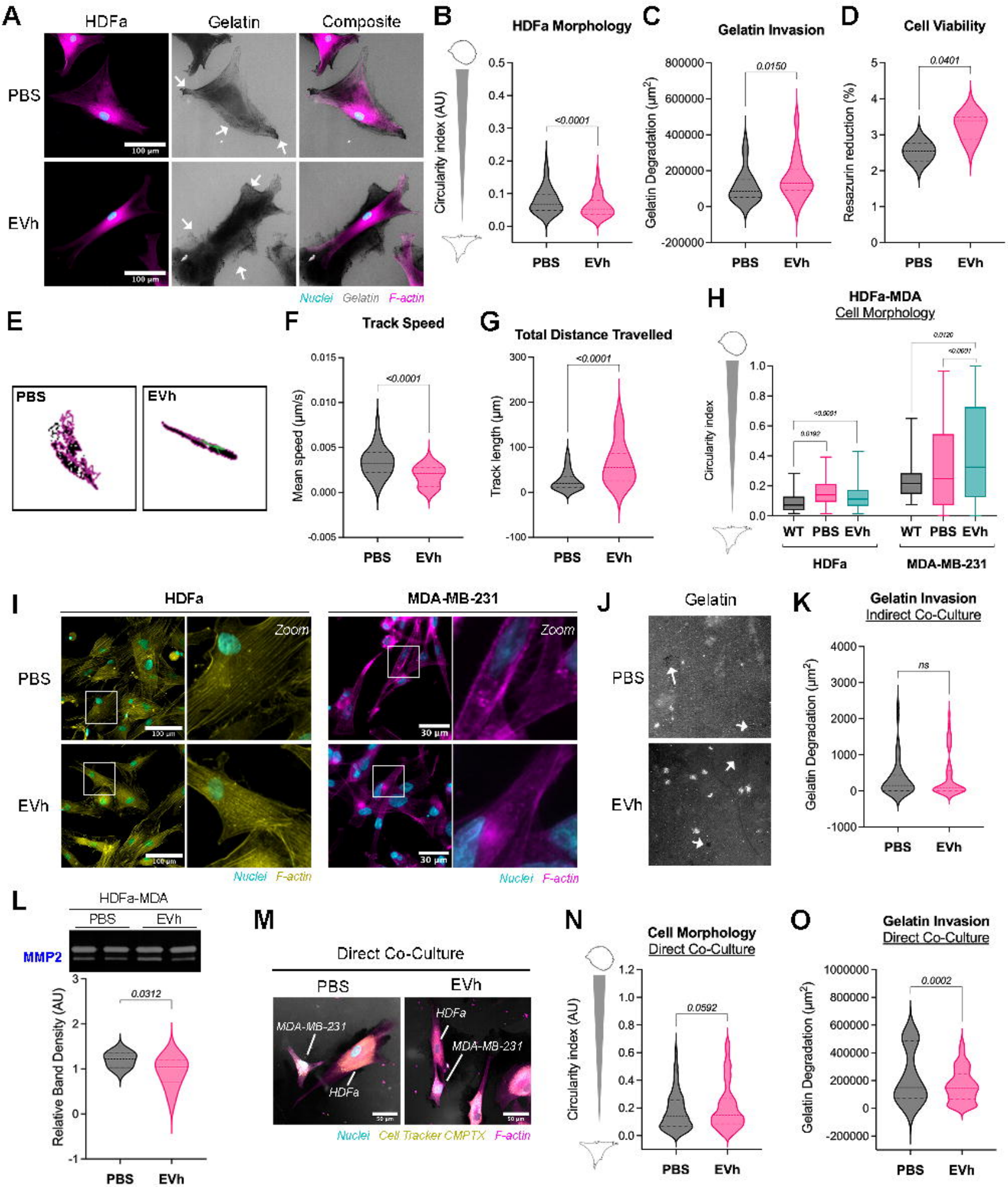
A
HDFa
Gelatin
Composite
PBS
EVh
100 µm
Nuclei Gelatin F-actin
B
HDFa Morphology
Circularity index (AU)
<0.0001
PBS
EVh
C
Gelatin Invasion
Gelatin Degradation (µm²)
0.0150
D
Cell Viability
Resazurin reduction (%)
0.0401
E
PBS
EVh
F
Track Speed
Mean speed (µm/s)
<0.0001
G
Total Distance Travelled
Track length (µm)
<0.0001
H
HDFa-MDA
Cell Morphology
Circularity index
WT PBS EVh
HDFa
MDA-MB-231
I
HDFa
MDA-MB-231
Zoom
30 µm
Nuclei F-actin
J
Gelatin
K
Gelatin Invasion
Indirect Co-Culture
Gelatin Degradation (µm²)
ns
L
HDFa-MDA
MMP2
Relative Band Density (AU)
0.0312
M
Direct Co-Culture
MDA-MB-231
HDFa
Nuclei Cell Tracker CMPTX F-actin
N
Cell Morphology
Direct Co-Culture
Circularity index (AU)
0.0592
O
Gelatin Invasion
Direct Co-Culture
Gelatin Degradation (µm²)
0.0002

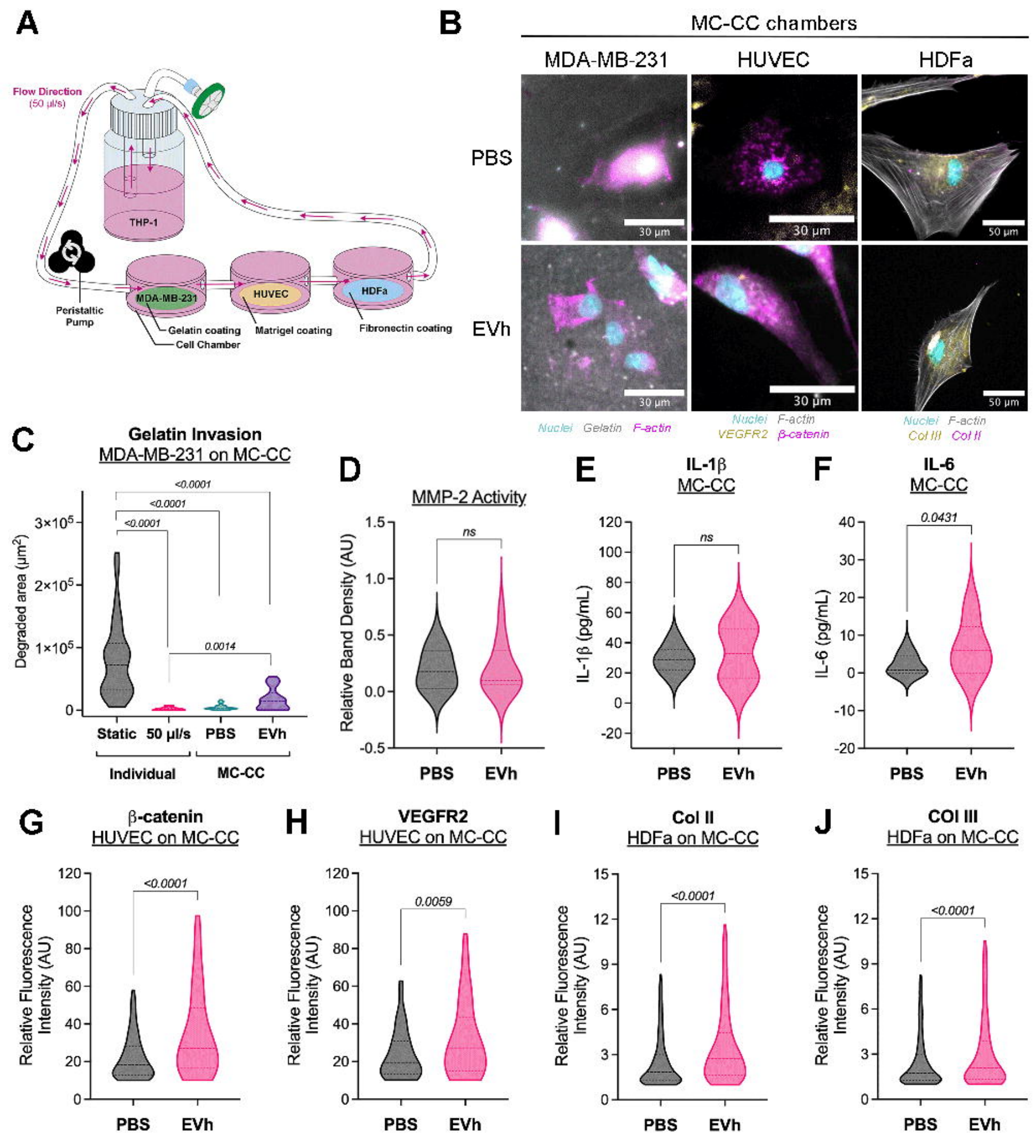
A
Flow Direction
(50 µl/s)
THP-1
Peristaltic Pump
MDA-MB-231
HUVEC
HDFa
Gelatin coating
Cell Chamber
Matrigel coating
Fibronectin coating
B
MC-CC chambers
MDA-MB-231
HUVEC
HDFa
PBS
EVh
30 µm
50 µm
Nuclei Gelatin F-actin
Nuclei F-actin VEGFR2 β-catenin
Nuclei F-actin Col III Col II
C
Gelatin Invasion
MDA-MB-231 on MC-CC
Degraded area (µm²)
3×10⁵
2×10⁵
1×10⁵
0
<0.0001
<0.0001
<0.0001
0.0014
Static
50 µl/s
PBS
EVh
Individual
MC-CC
D
MMP-2 Activity
Relative Band Density (AU)
ns
PBS
EVh
E
IL-1β
MC-CC
IL-1β (pg/mL)
ns
PBS
EVh
F
IL-6
MC-CC
IL-6 (pg/mL)
0.0431
PBS
EVh
G
β-catenin
HUVEC on MC-CC
Relative Fluorescence Intensity (AU)
<0.0001
PBS
EVh
H
VEGFR2
HUVEC on MC-CC
Relative Fluorescence Intensity (AU)
0.0059
PBS
EVh
I
Col II
HDFa on MC-CC
Relative Fluorescence Intensity (AU)
<0.0001
PBS
EVh
J
COl III
HDFa on MC-CC
Relative Fluorescence Intensity (AU)
<0.0001
PBS
EVh

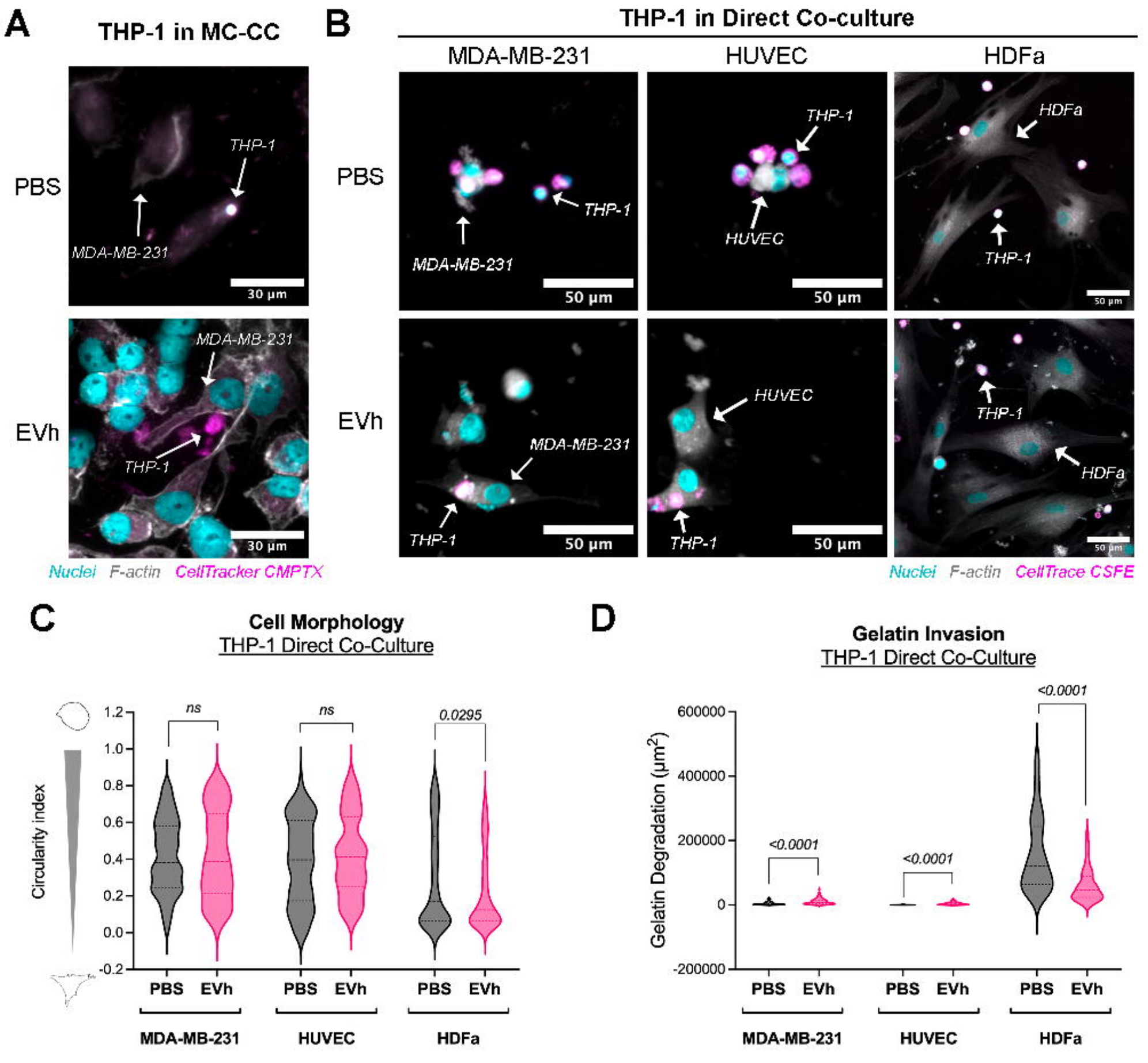
A
THP-1 in MC-CC
PBS
EVh
THP-1
MDA-MB-231
30 µm
Nuclei F-actin CellTracker CMPTX
B
THP-1 in Direct Co-culture
MDA-MB-231
HUVEC
HDFa
50 µm
Nuclei F-actin CellTrace CSFE
C
Cell Morphology
THP-1 Direct Co-Culture
Circularity index
ns
0.0295
PBS
EVh
D
Gelatin Invasion
THP-1 Direct Co-Culture
Gelatin Degradation (µm²)
<0.0001